Solar Energy Materials & Solar Cells 233 (2021) 111384

Contents lists available at ScienceDirect

Solar Energy Materials and Solar Cells

journal homepage: www.elsevier.com/locate/solmat

Prototype design and development of low-load-roof photovoltaic modules for applications in on-grid systems

Piotr Grygiel [a,b,*], Jan Tarłowski [b], Marta Prześniak-Welenc [c], Marcin Łapiński [c], Jacek Łubiński [d], Aleksandra Mielewczyk-Gryń [c], Krzysztof Mik [e], Michał Bartmański [d], Daniel Pelczarski [a], Maciej Kwiatek [d]

[a] Institute of Physics and Applied Computer Science, Faculty of Applied Physics and Mathematics, Gdańsk University of Technology, Narutowicza 11/12, 80-233, Gdańsk, Poland
[b] Xdisc S.A., Jagiellońska 82, 03-301, Warsaw, Poland
[c] Institute of Nanotechnology and Materials Engineering and Advanced Materials Centre, Faculty of Applied Physics and Mathematics, Gdańsk University of Technology, Narutowicza 11/12, 80-233, Gdańsk, Poland
[d] Faculty of Mechanical Engineering and Ship Technology, Gdańsk University of Technology, Narutowicza 11/12, 80-233, Gdańsk, Poland
[e] Energy Conversion and Renewable Resources Research Centre, Polish Academy of Sciences, The Szewalski Institute of Fluid-Flow Machinery Polish Academy of Sciences, Fiszera 14, 80-231, Gdańsk, Poland

ARTICLE INFO

Keywords:
Lightweight PV module
Prototype
Low-load capacity roof
On-grid systems

ABSTRACT

Four prototypes of lightweight photovoltaic modules for applications in on-grid systems have been designed, developed, manufactured and tested for compliance with relevant IEC standards. Selected, commercially available materials characterized by thermogravimetry, differential scanning calorimetry, dilatometry, scanning electron microscopy and nanoindentation technique were used in frameless, adhesively-bonded sandwich-structures carrying the interdigitated back contact solar cells. With dedicated manufacturing processes the prototype-dependent weight between 3.37 and 3.77 kg/m^2, the STC-maximum power in the range of 221–239 Wp together with power conversion efficiencies of 19.98–20.71% were obtained. Millimetre-sized texture improved module's performance for steeper solar incidence angles. The self-cleaning capability of modules was enhanced by a hydrophobic material utilized in front linings. The structure of the prototypes helps to build non-intrusive installations on low-load capacity roofs, even in large-scale lightweight buildings.

1. Introduction

The share of electricity in global energy consumption is expected to rise from 19% in 2018 up to 24% in 2040 or even 31% provided that the Sustainable Development Scenario (SDS) is introduced. Up to 75% of renewable contribution to overall energy supply should occur in 2040, suppressing coal by the year 2026. Assuming realization of the SDS, by 2040 the renewables will provide 75% of the global electricity, with the share of solar photovoltaic (PV) and wind systems as high as 40% [1].

Among renewables, the PV systems have become widely used during the past decades. For instance, between 2010 and 2018 The Compound Annual Growth Rate of PV facilities was as high as 36.8% [2] and more than 40% over the last 10 years [3]. Regarding the world's PV power capacity, levels of 1.2 TW in 2022 [4] and 1.4 TW in 2024 have to exceed 4 TW by 2025 and 21.9 TW by 2050 [3] to achieve the carbon-free energetics. It means for the European Union that the capacity must increase to 0.63 TW by 2025 and 1.94 TW by 2050 [3].

Photovoltaics produces electricity in various geographical locations and is easy scalable for medium/small businesses and households. Here, the economic benefits are crucial. For all commercial technologies the price learning curve shows module price declining from ca. 30 €$_{2018}$/Wp in 1980 to ca. 0.5 €$_{2018}$/Wp in 2015 [2]. The trend continues, so by year 2019 the PV module spot prices of ca. 0.22 USD$_{2019}$/Wp (approx. 0.2 €$_{2019}$/Wp) were reported [3].

* Corresponding author. Institute of Physics and Applied Computer Science, Faculty of Applied Physics and Mathematicsf, Gdańsk University of Technology, Narutowicza 11/12, 80-233, Gdańsk, Poland.
E-mail addresses: piotr.grygiel@pg.edu.pl (P. Grygiel), jan.tarlowski@x-disc.pl (J. Tarłowski), marta.welenc@pg.edu.pl (M. Prześniak-Welenc), marcin.lapinski@pg.edu.pl (M. Łapiński), jacek.lubinski@pg.edu.pl (J. Łubiński), aleksandra.mielewczyk-gryn@pg.edu.pl (A. Mielewczyk-Gryń), kmik@imp.gda.pl (K. Mik), michal.bartmanski@pg.edu.pl (M. Bartmański), daniel.pelczarski@pg.edu.pl (D. Pelczarski), maciej.kwiatek@pg.edu.pl (M. Kwiatek).

https://doi.org/10.1016/j.solmat.2021.111384
Received 17 June 2021; Received in revised form 13 August 2021; Accepted 6 September 2021
Available online 17 September 2021

In this context, the presence of market niche becomes important. It regards lightweight buildings (production halls, supermarkets, farms, etc) with low-load capacity roofs of area being huge and difficult to estimate. Expensive reinforcement of such constructions is needed prior to fitting of heavy conventional PV systems. This could render projects uneconomical, both for new buildings and existing ones. Importantly, the structural design of the latter ones is usually on the brink of standard requirements. The lightweight modules can be mounted using fixings as for conventional PV systems or bonded directly by adhesives which is known as building attached photovoltaics (BAPV) [5]. Note that building integrated photovoltaics (BIPV) replaces conventional elements of building envelope with structures containing PV devices which is the substantial difference between BAPV and BIPV.

Therefore, high-efficiency modules are required with the weight reduced from the current ranging between 12 and 20 kg/m^2 (see Ref. [6] and references therein), with contributions of glass plates and aluminium frames estimated at, respectively, 69% and 11% [7]. In lightweight constructions these elements are eliminated and PV cells are sandwiched between polymeric front- and backsheets, as e.g. in devices used in PV-powered recreation boats [8].

The concept of modules' multilayer architecture was the subject of extended investigations. Particularly, the following papers [6,9–11] deal with structures consisting of two main components: composite backsheets (skins/sandwich-adhesive/core) and frontsheets (encapsulant/PV-cells/polymeric frontsheet). As sandwich adhesives the EVA, ionomer and polyolefin films were used. Aramid and aluminum honeycomb sheets were utilized as the cores. It should be noted that small (single- and double-cell) and medium-area (12 and 16-cells) modules have been studied, with reported structure mass (including frame) of about 6.5 kg/m^2 [6] and about 5 kg/m^2 [9]. Those structures were successfully subjected to selected (thermal cycling, damp-heat and hail resistance) aging tests imposed by IEC 61215–2:2016 industrial procedure. Another sandwich-structure was studied in Ref. [12]. The Authors proposed laminated layers of polyvinyl fluoride, polyethylene terephthalate, EVA together with EVA- or non-EVA encapsulants. A somewhat different concept of replacing a standard glass cover with a thin acrylic layer was suggested in the work [13]. Such a solution allowed for a weight reduction of 46% compared to the standard module. Two types of structures were investigated: with an acrylic film used as the front- and backsheet (plastic sheet PV module) and an acrylic film as the frontsheet, with a glass-epoxy plate as the backsheet (plastic film PV module). The single- and four-cell minimodules were investigated. Particularly, the thermal cycling, humidity, freezing and damp-heat tests according to IEC 61215 standard were positively performed. The modules' impact resistance was also successfully examined by means of a steel ball dropping (a substitute for the hail test). It should be noted that the four-cell modules were supported on an aluminum frame. A concept of a light module structure with a PV cell sandwiched between polycarbonate layers was presented in the paper [14]. The residual post-lamination stresses in the cells were investigated analytically and by means of the finite element technique. As shown, the residual stresses within the silicone PV modules are highly compressive which, interestingly, enabled the fabrication of minimodules having a significant curvature, as under such conditions the semiconductor material is protected against cracking when subjected to bending. A multi-layered structure based mainly on polyester foam has been developed [15] providing more than 50% of standard module weight reduction.

Bearing in mind the market expectations, we decided to design, develop, produce and test four prototypes of innovative, lightweight photovoltaic modules for applications in on-grid PV systems. As a basic concept for the study an adhesively-bonded, frameless construction was chosen with a ribbon-interconnected cell matrix sandwiched between the frontsheet and encapsulating layers, this structure being set-up on a composite backsheet. For the future profitable production and due to module safety requirements, the application of commercially available components was adopted.

To achieve these goals the following studies were performed: characterization of construction materials, design of module constructions, development of production process, tests of module performances and power optimization of the cells for the prototypes. Regarding potential solutions for lightweight PV devices known from the literature above, one has to emphasize that the results of works on the designing/manufacturing technology of small- and medium-scale modules cannot be directly related to the standard-sized devices. Indeed, the production of standard modules requires solving technical and technological issues which might not occur for low-dimensional structures. Those are related e.g. to technology of numerous electrical connections, effective lamination (with an acceptable number of flaws in accordance with IEC test standards) and mechanical reliability. Therefore, refinements of the developing/production processes are necessary due to the specificity of full-size device manufacturing. Indeed, in Ref. [16] a numerical simulation of stresses in PV cells in a full-sized (66-cell) module was performed as an extension of a previous work on one-cell device. As an example of the "small-full-size" issue, one can give that of deformation under load of modules with a thin acrylic layer being raised in the paper [13] which turned out to be insufficient for standard devices.

With dedicated production processes, selected construction materials and PV cells the following requirements were set: minimum efficiency of 19%, maximum total weight of 3.5 kg/m^2, electrical power exceeding 200 Wp and hydrophobic front-covers with minimal wetting angle of 100°. To enhance the performance for steeper solar incidence angle, utilization of a low-cost technique of light management was assumed. All prototypes were expected to comply with applicable IEC reference standards.

Regarding the production process of PV modules, adhesion of construction materials is one of the basic issues that must be solved to achieve their durability and resistance to weathering. Therefore, the issue of reliable adhesion measurement becomes crucial and implies the necessity to look for alternative techniques to the currently used methods, e.g. the peel-test. Indeed, in Ref. [17] a simple technique of adhesion measurements was proposed. The adhesion is not convoluted with material bulk deformation and a single critical load measurement of the sample is performed. With this technique, the Authors showed that, as compared to new modules, the encapsulants' adhesion in the devices after 27 years of field work (direct exposure to solar radiation) was even more than 90% and for backsheet adhesion – up to 98% lower. The delamination becomes specific in the case of particularly demanding environmental conditions (very humid climate in tropical and coastal regions), i.e. exposure to salt mist, water vapour and acid penetration. The adhesion degradation process between the encapsulant and the backsheet was investigated by a method based on fracture mechanics in which the adhesive energy was measured as described in Ref. [12]. Another point of interest are the stresses that are induced in PV cells during module production. Residual stresses in the cells do depend on the course of the lamination process. In paper [16] numerical simulations employing the finite element modelling of stress evolution in PV cells were conducted. Subsequent steps of an entire manufacturing cycle of a conventional laminate were analysed to determine the accumulated final residual stresses. It has been concluded that the stresses occurring during the lamination's pressure-ramping are the most critical and the stresses are weaker for thinner cells. The cells' post-lamination residual stresses are also examined in Ref. [14]. This paper deals with such stresses as modelled (by means of finite-element and analytical techniques) for a lightweight polycarbonate/cell/polycarbonate structure. Accordingly, the stresses are highly compressive which inhibits the increase of cell cracking. This allowed the production of minimodules of significant curvature that is important for the development of lightweight PV devices.

To sum up, the present paper concerns light structures of frameless PV modules with refined manufacturing technology. As an extension of the small-scale investigations known from the literature, it can be useful for those who design and prepare production of such structures of

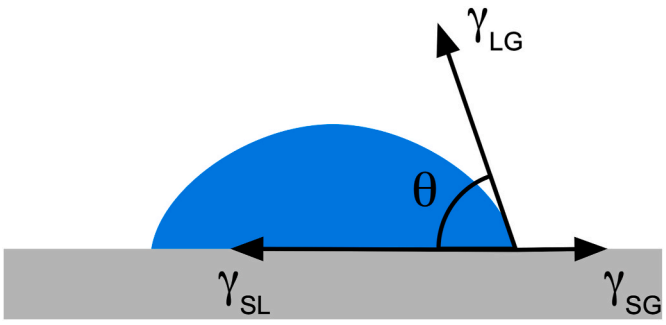

Fig. 1. Interfacial tensions for a liquid droplet on a smooth surface.

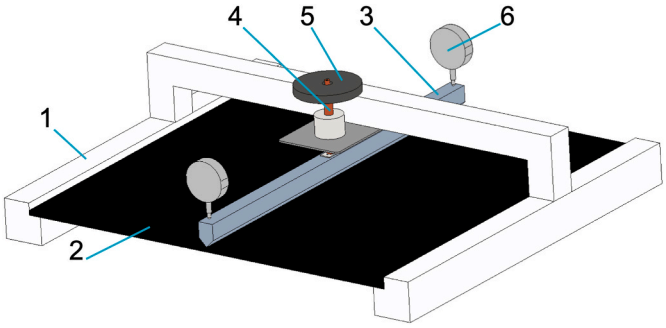

Fig. 2. Test bed for Young's modulus determination of substrate cores by bending.

standard size. To our knowledge, such a type of various, full-size constructions tested in accordance with the full-cycle of IEC procedures, which constitute a potential market offer, have not been the subject of a single paper so far.

2. Measuring techniques and methodology

2.1. Material and module characterization

The **water repellency of module outer layers** was determined by measurements of the water contact-angle, θ, using the sessile-drop-technique and the Young equation (see e.g. Ref. [18] and references therein):

$$\cos\theta = \frac{\gamma_{SG} - \gamma_{SL}}{\gamma_{LG}} \tag{1}$$

where γ_{SG}, γ_{SL} and γ_{LG} are, respectively, the tensions at solid-gas (air), solid-liquid and liquid-gas interfaces (Fig. 1).

To obtain the **images of components of module sandwiches** an FEI Quanta FEG 250 scanning electron microscope (SEM) with 10 kV-acceleration voltage and secondary-electron detection was used.

Thermal behaviour of materials for module structures was examined by applying thermogravimetric analysis (TGA), differential scanning calorimetry (DSC) and dilatometric (DIL) technique. The TGA was conducted using a NETZSCH TG 209 F3 Tarsus® microbalance. Open alumina crucibles were utilized to measure samples of identical weight (10 ± 1 mg) in synthetic air at temperatures between 30 and 450 °C with the heating rate of 10 °C/min. The first derivative of TGA (DTG) was calculated using Netzsch Proteus ThermalAnalysis program. The DSC was performed using a NETZSCH DSC 204 F1 Phoenix® calorimeter. Closed sample alumina crucibles were applied, the temperature ranged between 30 and 240 °C with other conditions as for the TGA measurements. The coefficient of thermal expansion (CTE) of samples and their relative changes in length were examined using a Netzsch DIL 402 PC dilatometer in an argon ambient atmosphere between 30 and 160 °C at a constant heating/cooling rate of 0.5°C/min. The shielding atmosphere was obtained by a 50 ml/min-rated flow of argon. The 25 mm × 8 mm-sized samples were examined to determine the $L = f(T)$ curves with L and T denoting, respectively, the sample length and temperature. The linear CTE was calculated by the formula

$$\propto = \frac{\Delta L}{L_0}\frac{1}{\Delta T} = B \tag{2}$$

with $\Delta L/L_0$ – the relative change in sample length (of initial length L_0) due to a change in its temperature of ΔT and B – the slope of the function $dL/L_0 = f(T)$.

Mechanical properties of elements of module structures were determined using nanoindentantion technique (front-covers) and static-bending method (the cores of rear-covers). A NanoTest™ Vantage, Micro Materials system with a diamond, three-sided pyramid Berkovich indenter of a 124.4° vertex angle was utilized. A series of 25 three-stage indentation procedures was conducted at ambient temperature. At first, the load increasing from 0 to 5 mN at a rate of 0.25 mN/s rate was applied to the sample, this being followed by a 5 s-maximal-load-holding period. Finally, the load on the indenter was released at the rate of 0.25 mN/s. Indentations' spacing was set at 20 μm along both axes. Based on measurements the reduced Young's modulus, E^*, and the hardness, H, of the front layer were calculated by Oliver–Pharr method [19]. The maximum depth of the indenter deflection, h, the plastic, W_{Plast}, and elastic, W_{Elast}, layer deformation works were also determined. The substrate cores' Young modulus was measured in a static bending experiment using set-up shown in Fig. 2.

A rigid frame (1) was built to house the specimen (2) and support it along opposite edges. A prismatic load bar (3) was positioned across the specimen's centreline and connected to a push-rod (4), transferring load from dead-weight (5) to the specimen. Square (500 × 500 mm) specimens were used. Downward deflection was measured using dial gauges (6) at load bar's ends. The force was progressed from 0 to 73 N in 7 steps and then regressed in the same manner. Measurements were taken at every load stage. The procedure was repeated 5 times for longitudinal and transverse specimen orientation. The Young's modulus was evaluated from the formula:

$$E = \frac{Fb^3}{48sI} \tag{3}$$

with F – the downward force (load), b – specimen span between support edges, s – downward specimen deflection, I – geometric moment of inertia of the specimen's cross-section.

Performance of module front-cover textures was assessed in indoor measurements on A4-sized modules with a single 156 × 156 cm 4 bus-bar Si-monocrystalline cell to avoid the manufacturing of full-sized devices. Such technique was used in papers regarding glass-covered module constructions [20–22]. The cells were laminated between front covers and white 1 mm-thick epoxy-glass sheets, with soldered solar ribbons accomplishing electrical connections. A 1000 W/230 V AC halogen photo-reflector was used as a light source, with a holder that allowed tilting the modules between 0° (perpendicular direction) and 90° at 5° increments. The module's maximum power point, P_{mp}, was calculated from the current-voltage characteristics measured using a Gamry Interface 1000™ potentiostat/galvanostat/ZRA device. Due to the instrument maximum range limit, the sample illumination was set to (100 ±2) W/m^2 by adjusting the sample-reflector distance being large enough to effectively stabilize the sample temperature. The relative P_{mp} angular dependencies were determined with reference to the data for non-textured modules, which was found to be sufficient for assessing the performance of textures. Three samples of each texture type were examined for cell polarising voltage ranging from 0 to 0.55 V with respect to the illuminated electrode.

To examine the **applicability of lamination process stages** the 180° peel tests according to the ASTM D3330 standard were conducted. Electroluminescence (EL) tests were also performed to detect electrical

Table 1
Optical and environmental characteristics of the components together with results of nanoindentation of the front-cover structure for all prototypes: the reduced Young's modulus, E^*, the layer hardness, H, the maximum depth of the indenter deflection, h, the plastic deformation work, W_{Plast}, and the elastic deformation work, W_{Elast}.

Component composition	Manufacturer/Brand Name	Thickness (μm)	Remarks/notation in the text
ETFE + PV inside coating	Aluminium Féron/HelioX PV® frontsheet transluX EC 100	100	Outer layer/Féron frontsheet
EVA	STR®/Photocap® 15585/P/UF/HLT™	450 or 200, prototype-depending	Encapsulant/Photocap® encapsulant
Optical and environmental characteristics, test methods			
ETFE film/product[a]			
Solar transmittance of ETFE film (%)	93	DIN EN 410/AM1 global, 300–2500 nm[b]	
Artificial weathering (h)	12 000	ISO 4892-2/method A, cycle 1	
Damp-heat test (h)	min. 2000	IEC 61215/85 °C, 85% RH	
Humidity-freeze test (cycles)	min. 30	IEC 61215/-40 °C -> 85 °C, 85% RH.	
EVA[c]			
Optical transmission (%)	91	ASTM E424/23 °C, 460 μm thickness, AM2, 350–2500 nm[b]	
UV cut-off wavelength (nm)	360	ASTM E424/23 °C, 460 μm thickness, AM2, 350–2500 nm	
Refractive index	1.48	ASTM D542/23 °C, 460 μm thickness, AM2, 350–2500 nm[b]	
Water absorption (wt%)	<0.1	ASTM D570	
MVTR (g/m^2/day)	18	ISO 4892-2/method A, cycle 1	
Results of front-cover structure nanoindentation			
E (MPa)	H (MPa)	h (nm)	W_{Plast} (nJ)	W_{Elast} (nJ)
197 ± 4	22.6 ± 0.5	3628 ± 28	3.68 ± 0.06	4.64 ± 0.07

Data taken from:[a][34],[b][35],[c][36].

inhomogeneities of the solar cells and cell interconnections (see e.g. Ref. [23]). An Ecoprogetii KEL-1600 EL tester was utilized.

To **optimize the single-cell power** for module efficiency ensuring the cost-effective production, the Cell-To-Module (CTM) gains and losses analysis [23] was performed, according to the formula

$$\mathrm{CTM} = \frac{P_{\mathrm{mp}}}{\sum_{i=1}^{N} P_{\mathrm{ci}}}. \tag{4}$$

Here P_{mp} regards the module in statu nascendi and $\sum_{i=1}^{n} P_{\mathrm{ci}}$ is the total maximum power of N cells applied. The optimized power of a single cell was then determined:

$$P_{\mathrm{c,o}} = \frac{P_{\mathrm{mp,\eta}}}{N \times \mathrm{CTM}} \tag{5}$$

where $P_{\mathrm{mp,\eta}}$ is the maximum power of the module with required, cost-effective efficiency.

3. Prototypes design

During the production of multilayer structures with polymeric components, the interfaces between encapsulant/PV cells, interconnecting ribbons/encapsulant and encapsulant/backsheet are build-up. The interfacial interactions being driven by UV irradiation and other climate factors can lead to structural degradations, i.e. discolouration, encapsulant and/or backsheet delamination which results in power reduction and/or aesthetic and safety issues. The mechanisms involved are polymer-dependent and were extensively studied (see e.g. Ref. [24] and references therein). The modules' performance can further decrease due to mechanical stress and thermo-mechanical fatigue. The failures of PV modules have been reviewed and presented along with relevant statistics [25]. Accordingly, panel degradation can be effectively reduced/avoided by properly developed structure, application of compatible construction materials and careful development of production processes which are the subjects of the present study.

3.1. Front-covers

Apart from providing some structural support, optical coupling, electrical insulation and protection of interconnected PV cells from environmental degradation should be provided by a module front cover. Dirt deposition significantly reduces modules' performance degrading the cover transmittance and thermal management. Experimental outcomes obtained worldwide over last decades has been reviewed [26,27]. In that paper the maximum losses of PV modules' cover transmission up to 37%, the short-circuit current up to 42%, efficiency up to 60% and output power up to 55%, testing period were cited from outdoor soiling studies. These values depend, among others, on front surface, climate, environment and exposure period. Different dirt samples deposited on acrylic plastic and low-iron-glass surfaces of Si-monocrystalline module were used in an indoor-experiment [28]. Particularly, the degradation of short-circuit current by 9% (carpet dust), 12% (salt), 17% (coarse sand), 21% (cement), 30% (sandy soil) and 46% (bird droppings) was registered for the plastic cover. The degradation increased up to 72–95% for wet depositions on the surfaces. Considering the efficiency of rain-cleaning at exemplary locations, an annual loss of PV production was reported e.g. of ca. 3.6% in Mexico City, with an up to 15% reduction during more than 60-days rainless periods [29]. In Malaga, Spain, even a light rain recovered the performance of a glass-covered PV module below the average daily power losses of 4.4%, these losses exceeding 20% for long rainless periods [30]. Similarly, the 13% and 27% losses of the glass-covered module efficiencies were observed on the Canary Islands, Spain, i.e. directly at the Atlantic Ocean, also with a complete recovery due to precipitations [31]. In northern Poland (the city of Gdańsk) the ca. 25% module efficiency reduction per micrometre of dust-layer thickness was reported with natural cleaning being insufficient [32]. Anti-soiling effect can be achieved by water-repellent hydrophobic surfaces [23] which help the formation of water droplets and induce spontaneous removal of contaminants.

Therefore, combined polymer front-covers were chosen for the prototypes. The ability to self-clean was achieved by an Aluminium Féron frontsheet foil (Feron frontsheet – see Table 1) used as structures' outer layers. The water contact-angle $\theta = (107 \pm 6)^{\circ}$was obtained using formula (1) which defines the Féron frontsheet hydrophobicity [33].

From proper cover structures high volume-resistivity and the ability to form a strongly bounded laminate with other module components with sufficient shear stress compensation are expected. Nowadays, also due to its low cost, the copolymer ethylene vinyl acetate (EVA) is commonly used in the PV industry in wafer-based modules. For these reasons, apart from the hydrophobic Féron frontsheet the STR® Photocap® encapsulation foil (Photocap® encapsulant – see Table 1) was utilized to form the laminated front layers on all prototypes. For effective optical coupling of PV cells, high transparency for spectral range of 380–1100 nm and an optimal refractive index should be provided by a cover structure [23]. As seen from the producers' data of Table 1, the application of industrial PV-dedicated materials does meet these

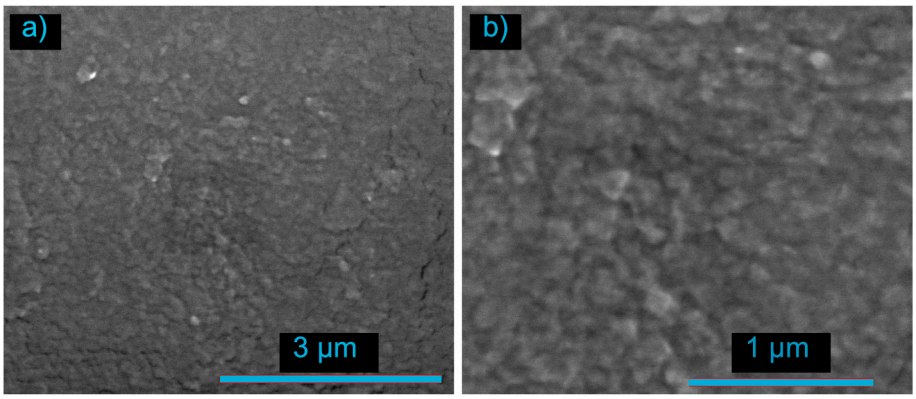

Fig. 3. SEM images of the Féron frontsheet/Photocap® encapsulant foil laminate surface with magnification of (a) 20 000 × and (b) 50 000 × .

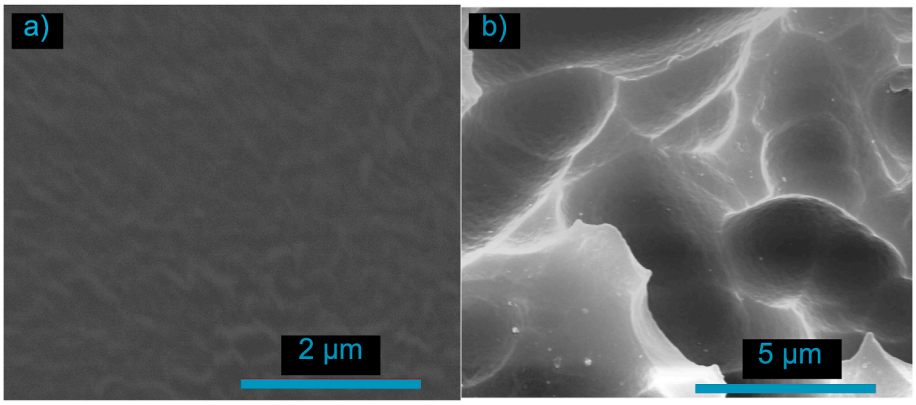

Fig. 4. SEM-imaged surface of the Féron frontsheet/Photocap® encapsulant/PV Si polycrystalline cell sandwich (a) and of an uncoated cell (b).

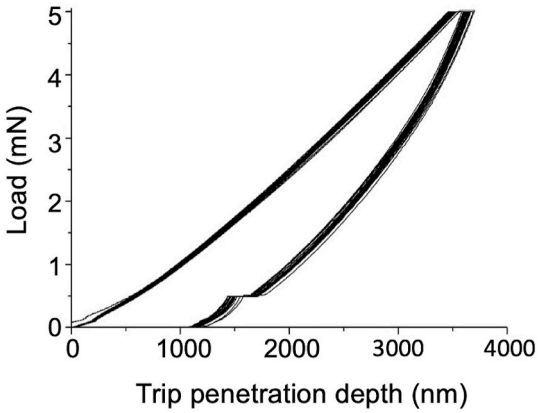

Fig. 5. Load-displacement curves of the Féron frontsheet/Photocap® encapsulant laminated foil.

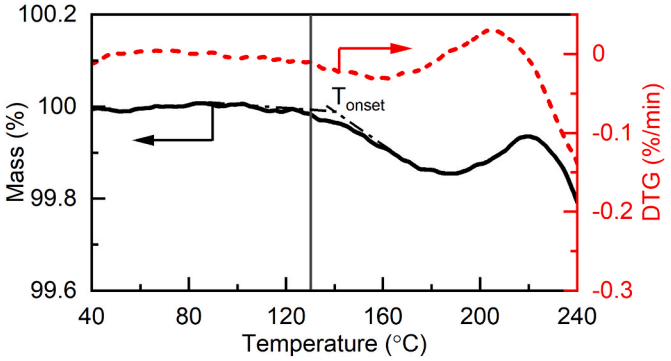

Fig. 6. TG and DTG curves of the Féron frontsheet/Photocap® encapsulant laminated foil.

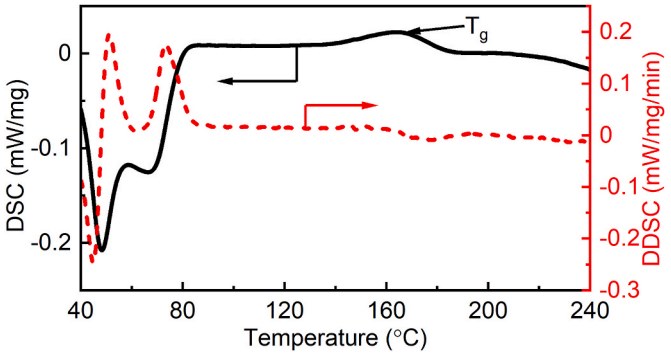

Fig. 7. DSC and DDSC curves of the Féron frontsheet/Photocap® encapsulant laminated foil.

requirements. With lamination parameters not deviating from those typical and acceptable by the manufacturers, the optical features of front-covers were as given by the producers. Indeed, a few-percent variation in transmission of various EVA films laminated at temperature range of 90–175 °C was reported [37,38] with one-tenth change in refractive index [38].

Polymer materials are vulnerable to environmental factors. Regarding the front-covers, their discolouration (yellowing) and delamination are crucial for modules' performance losses. According to manufacturer's data [34] the outer front-covers' component (ETFE + PV inside coating – see Table 1) was subjected to artificial weathering tests involving a 12 000-h exposure to light of a xenon-source with spectrum containing a UV component. No significant changes in colour, yellowing, gloss nor adhesion were observed. Similarly, the damp-heat and

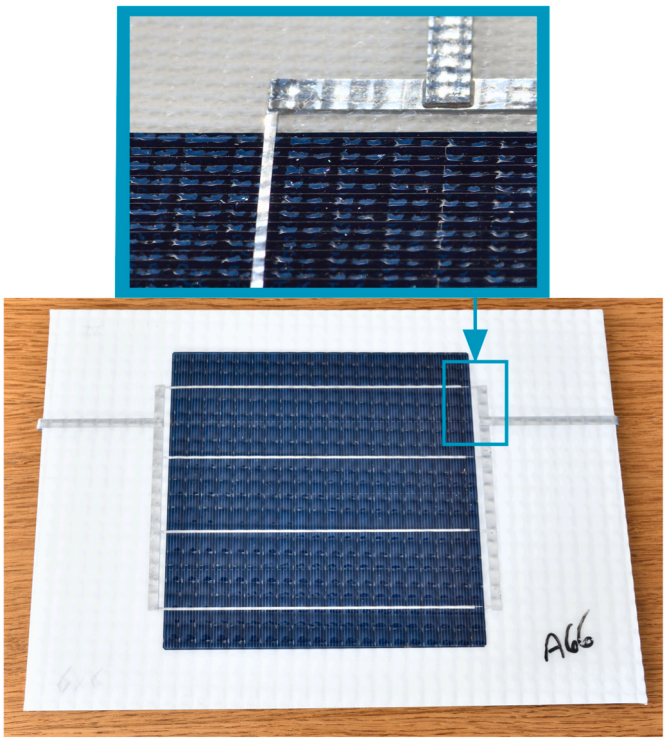

Fig. 8. An exemplary single-cell module with 6 mm-sized mesh texture.

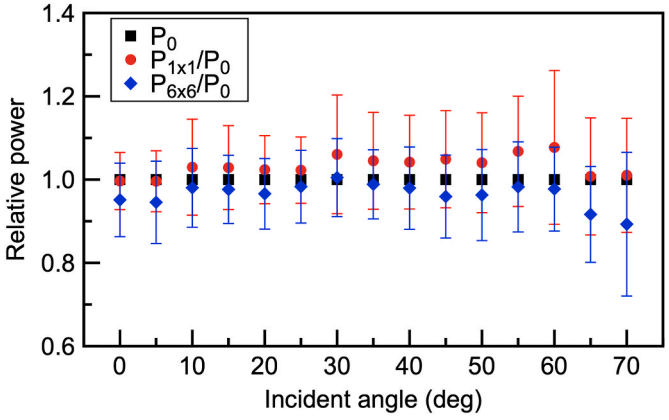

Fig. 9. Angular dependencies of maximum power for single-cell modules for the best (1 × 1 mm-sized, $P_{1\times1}$) and the worst (6 × 6 mm, $P_{6\times6}$) performing textures (P_0 relates to untextured samples).

humidity-freeze tests (performed on laminated modules) showed no significant changes in parameters, including adhesion to the encapsulation film. On the other hand, extended investigations of EVA were reported, concerning the degradation mechanisms and processing effects on its stability [39–41] and the climate/environmental aging [42, 43]. Accordingly, a reduction of performance is to be expected for the modules long-time operating in field conditions. For instance, apart from discolourations, up to ca. 24% decrement in output power was reported for devices naturally (in-field) aged for over 22 years [44]. We refer to this problem in this paper's conclusions.

To examine the applicability of the frontsheet/encapsulant films, SEM-imaging tests of the structure were performed on laminated samples. Corresponding results are depicted in Fig. 3.

A homogeneous surface is seen, free from major flaws, with ca. 100 nm-structures visible at 50 000× magnification. Since the Si-PV cells were assumed for the prototypes, a polycrystalline cell was sandwiched between the front cover and a 3 mm-thick polycarbonate backsheet and examined using SEM technique. Resulting image of a homogeneous, flawless surface is shown in Fig. 4a together with that of an uncoated cell (Fig. 4b). Therefore, the sufficient quality of the front covers can be expected with the materials used.

Since material parameters of the front-cover are crucial for the module response to environmental influence, the nanoindentation of the frontsheet/encapsulant layer was performed. Such a technique allowing the measurements' high spatial resolution was successfully applied in a study of hardness changes of the PV module encapsulant (EVA) and backsheet due to aging process [45]. Fig. 5 shows the load-displacement (the tip penetration depth) curves for subsequent indentations.

The curves of individual indentations exhibit a very narrow spread which confirms homogeneous mechanical properties of the sample. This is a desired module cover layer feature since the areas of heterogeneity are usually responsible for the initiation of destruction under the load. Table 1 shows the results of nanoindentation which predispose the material to be used in the flexible-by-design modules. Indeed, it should be ensured that the complete module can be easily deformed during assembly and operate in a deformed state (including significant cyclic relative deformations). This requires a relatively low value of reduced Young's modulus, E^*, the plastic, W_{Plast}, and elastic, W_{Elast} deformation works, i.e. high elastic deformation capacity. For operation at locations where abrasive material may be wind-carried at high speed, the module casing must be wear-resistant to suspensions of hard particles in air or water and to the effects of impingement by loose materials which also implies a low E^* and high deformability, with low value of H. Such a combination of mechanical properties is observed in rubber – one of the primary abrasion-resistant material. In fact, the values of H as high as 1 and 5 MPa were reported for silicon and natural rubber respectively, with W_{Plast} of ca. 20 nJ for both of them [46] together with the values of E between ca. 1 and 3 MPa for butyl rubber [47].

Table 2
List of composites for the prototypes' backsheet cores for together with bulk Young's moduli, E, from sample static-bending test – formula (3) – and thermal expansion coefficients, ∝ , from dilatometric measurements of the front cover/backsheet sandwiches. The ∝ of CF-N-CF and GF-N-GF could not be measured due to the flexibility of samples.

Manufacturer/Brand Name/notation in the text	∝ (× 10^{-6} K^{-1})	E (GPa)	Thickness (mm)	Prototype
MIKANIT/Nomex® HC carbon fibre laminate/CF-N-CF	–	15.55 ± 0.27[c] 13 ± 0.26[d]	5	P1
MIKANIT/Nomex® HC glass fibre laminate/GF-N-GF	–	8.42 ± 0.2[c] 6.45 ± 0.04[d]	5	P2
MASTERPLATEX/CF-Epoxy Platte HT/CFP	12.24 ± 0.02 (α_I)[a] 10.66 ± 0.05 (α_{II})[a] 2.97 ± 0.02 (α_I)[b] 21.16 ± 0.02 (α_{II})[b]	55[e]	1	P3
IZO-ERG/EPGC202 epoxy glass fibre laminate/EPGC202	10.4 ± 0.5 (α_I)[a] 5.29 ± 0.05 (α_{II})[a]	24[e]	1	P4

[a] sample heated up;[b]sample cooled down;[c]sample bent along x-axis;[d]sample bent along y-axis;[e]provided by the manufacturer: MASTERPLATEX E.K [52]. and IZO-ERG [53].

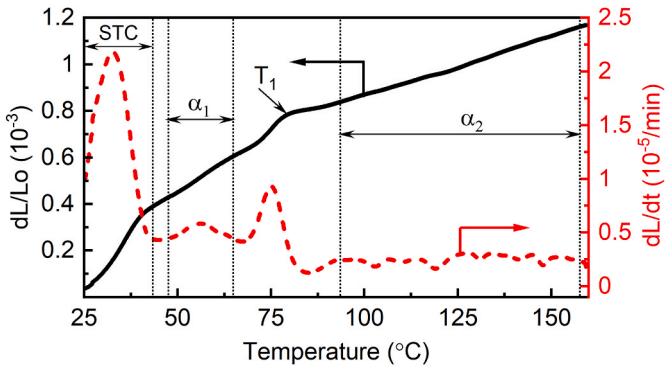

Fig. 10. The $dL/L_0 = f(T)$ function for the front-cover/EPGC202 sample.

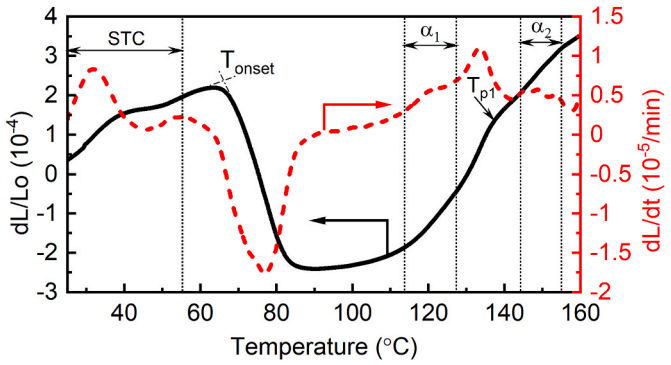

Fig. 11. The $dL/L_0 = f(T)$ function for the heated-up front-cover/CFP sample.

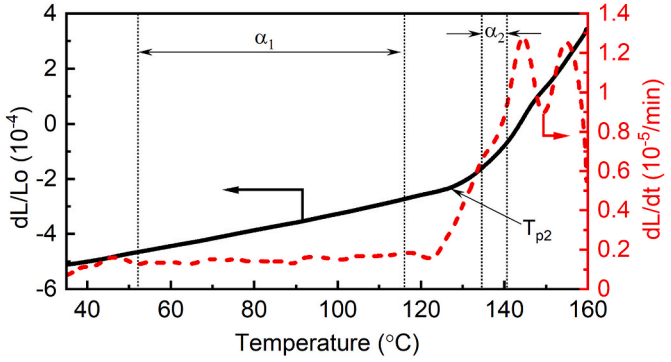

Fig. 12. The $dL/L_0 = f(T)$ function for the cooled-down front-cover/CFP sample.

Due to module operation at elevated temperatures, thermal stability of the layer was examined by thermogravimetric analysis (TGA) and differential scanning calorimetry (DSC). The TG and its first-derivative (DTG) curves are depicted in Fig. 6.

Since the sample's mass remains constant, its thermal stability is observed up to ca. 130 °C. Then, a process of material decomposition starts at T_{onset} = 144°C, beyond PV modules' operating temperatures. The DSC and its first derivative (DDSC) curves are shown in Fig. 7.

Firstly, a material transition from elastic to glassy state was detected at glass transition temperature, T_g = 166°C, again beyond the module's operational range. Two overlapping DSC minima for temperatures up to 90 °C, representing endothermic processes in the sample, were related to recrystallization of EVA, as reported in Ref. [48].

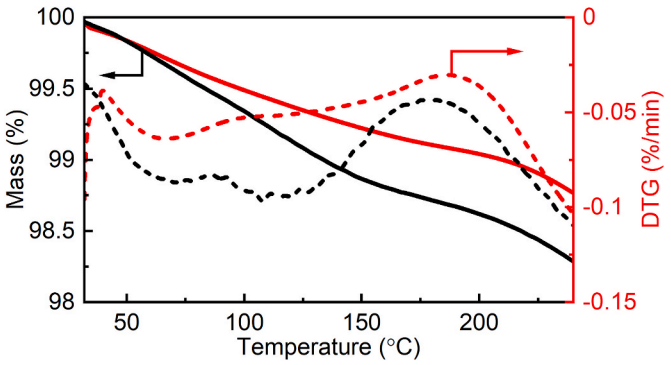

Fig. 13. TG and DTG curves (solid and dashed lines) obtained for CF-N-CF (black colour) and GF-N-GF (red colour) samples. (For interpretation of the references to colour in this figure legend, the reader is referred to the Web version of this article.)

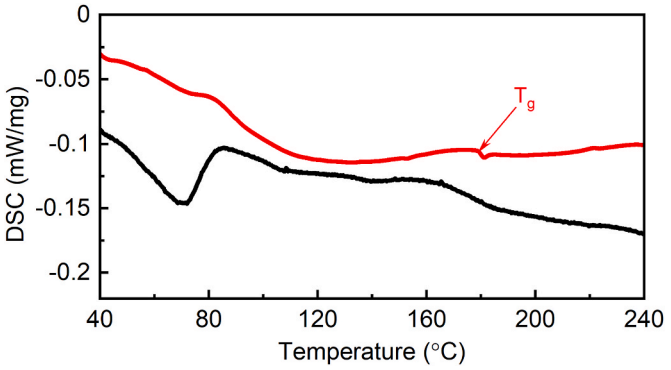

Fig. 14. DSC curves for CF-N-CF (black line) and GF-N-GF (red line) samples. (For interpretation of the references to colour in this figure legend, the reader is referred to the Web version of this article.)

3.2. Texturization of front-covers

Under field conditions, the non-perpendicular irradiation of PV panels will be predominant. Next, their frameless design is primarily not intended for tracking systems. To improve energy gain and achieve steeper incident irradiation angles anti-reflection coatings and/or different front-glass textures in frame-constructions were applied. The texture reduces the influence of air/front-cover interface and, through total internal reflection from it, also the light reflections from PV cells and the backsheet.

Applications of low-cost, commercial materials with millimetre-scale texture were reported in literature. Particularly, as compared to nominal power, P_{mp}, of monocrystalline-cell-based modules with non-structured glass, an increase of 1 and 1.5% was recorded with pits and inverted pyramids, with 3%-overall energy gain in Spain, can even be boosted by rising proportion of diffused light [22]. An over 3% increase in short-circuit current, I_{SC}, at STC was measured for heavy-textured (grooved) PV modules [20]. The efficiency increase of multicrystalline-cell-based modules between 2 and 8% at locations in Spain and Germany respectively, for chessboard-like grooved and deep pyramidal-patterned glass [49]. Later on, an increase of 2.7 and 2.9%, respectively for I_{SC} and P_{mp} (at STC) was reported for poly-crystalline Si-based modules (glass with inverted pyramids) as compared to untextured ones. These values correspond to two-year-term energy gain between 3.9 and 4.3% registered in the United Kingdom [50].

Due to the available manufacturing technology we decided to texturize the front covers by applying a simple square-mesh net during the lamination process resulting in cushion-shaped texture elements. The ARCs were not implemented as rather difficult to apply successfully

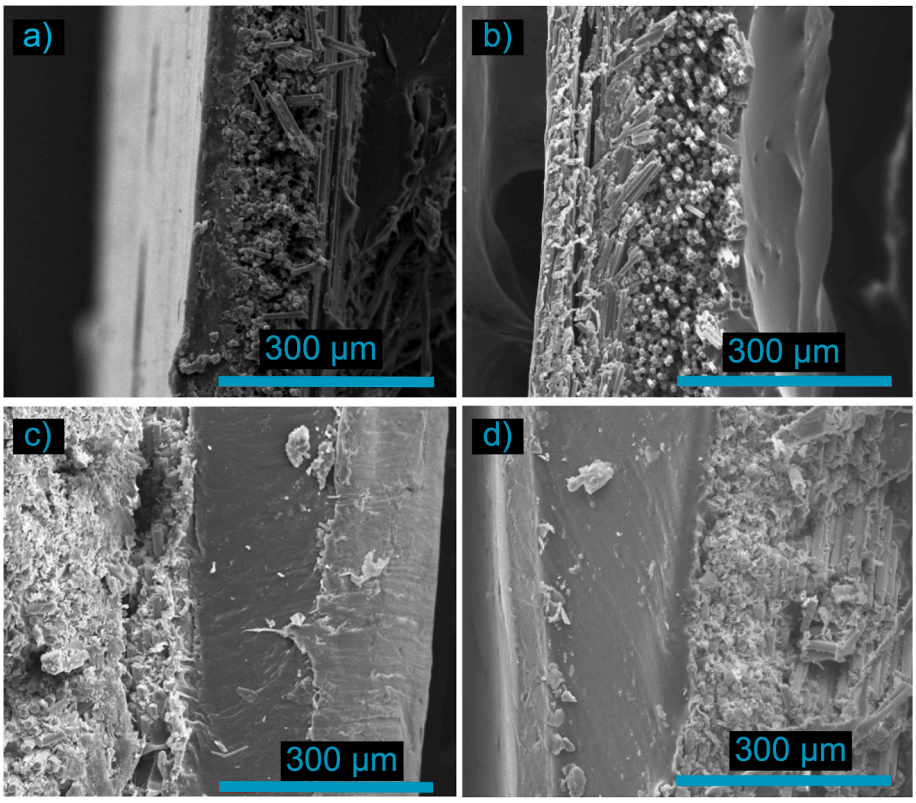

Fig. 15. SEM images of (a, b) Nomex®-CF and (c, d) Nomex®-GF interfaces with front-cover obtained before (a, c) and after (b, d) their heating up to 160°*C*.

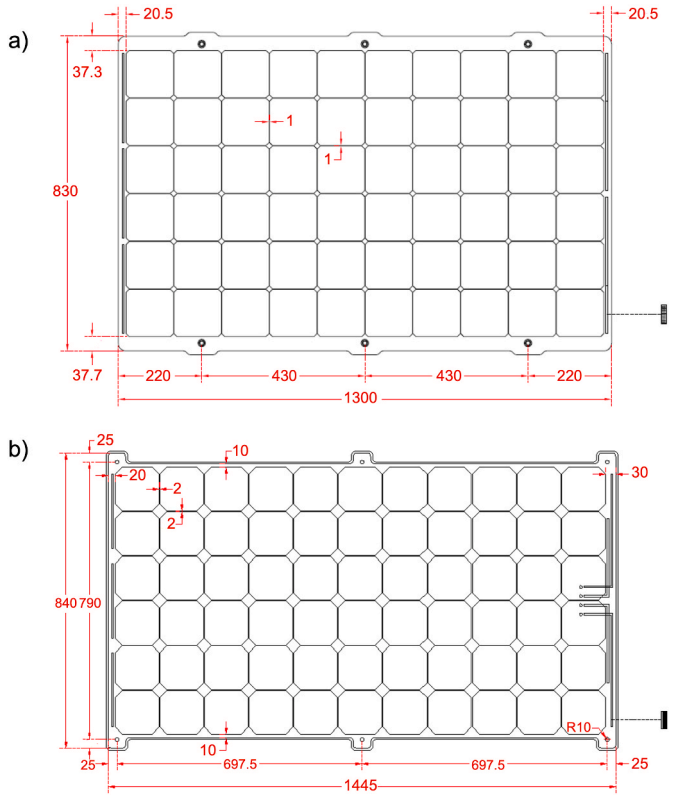

Fig. 16. Drawings of the prototypes: (a) P1 and P2, (b) P3 and P4 (active sides only).

to commercial polymeric materials, particularly on a production scale. The impact of texture sizing on P_{mp} of modules with front-covers of Section 3.1 was assessed in indoor measurements (cf. Section 2.1) using mesh-window of 1, 2, 4 and 6 mm in size (see Fig. 8) and can be deduced from Fig. 9.

For the sake of legibility, exemplary results (mean values of P_{mp} for three measuring series) for the best (1 × 1 mm) and the worst (6 × 6 mm) performing textures taken from Ref. [51] are plotted. As seen in Fig. 9, for the 1 × 1 mm texture the relative P_{mp} rises to ca. 9% for increasing incident angles of irradiation, but this value significantly drops for angles exceeding 60°. The steeper angles, however, have no practical importance due to the overall poor performance of modules for such illumination. The power gain decreased gradually for 2 and 4 mm gauge textures, down to values shown in Fig. 9. Consequently, the 1 × 1 mm texture has been chosen for all prototypes.

3.3. Rear-covers

Rear-covers (backsheets), apart from stability against solar radiation transmitted by front-cover, should provide durable adhesion and compatibility with panel encapsulant. Also, sufficient electrical insulation between the cell strings and the ground is mandatory to avoid safety issues, for assumed potential differences of 600 V. For low-weight and frameless structures of the modules, low-density materials of sufficient mechanical strength should be applied, to comply with the IEC 61215 standard. The composites selected as single-layer backsheet cores of prototypes named P1, P2, P3 and P4 are listed in Table 2.

An attempt was, therefore, made to apply more advanced multi-layer composites. In CF-N-CF and GF-N-GF sandwich panels a Nomex® HC honeycomb-core is lined with thin panels, respectively of carbon-fibre reinforced plastic laminate (CFRP) and of glass-fibre reinforced plastic laminate (GFRP), both epoxy resin based. The combination of high tensile/compressive strength of the outer layers and the lightweight core offers very high strength-to-weight ratio, especially in bending. In the

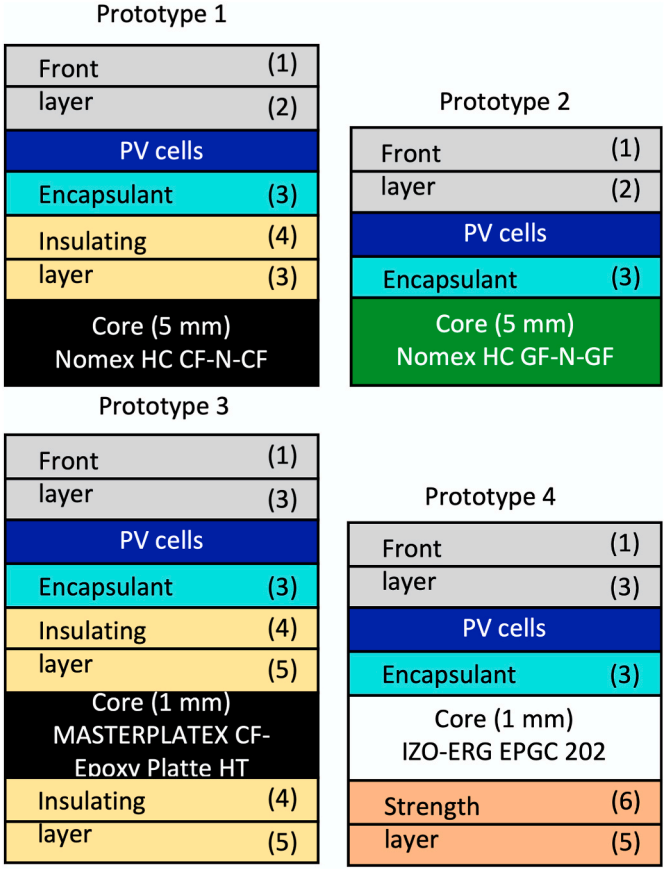

Fig. 17. The structures of the prototypes: (1) – 100 μm Aluminium Féron HelioX PV® frontsheet transluX EC 100, (2), (3) – STR® Photocap® 15585/P/UF/HLT™ EVA 450 μm (2), 200 μm (3), (4) – 170 μm Aluminium Féron Px 1000 insulation sheet, (5) – 50 μm Amcor Rayotec ECT50 (ECTFE), (6) – 200 μm STR® Photocap® 15580P/UF/HLT™ EVA.

CFP plates, individual carbon fibres are woven into a fabric, being later saturated with epoxy resin. This makes the material weight and rigidity superior to those of glass fibre-based composites. The downside is the low electrical resistivity of the order of several $\mu\Omega \times$ m [54] due to the properties of carbon fibres.

The PV modules are expected to withstand cyclic temperature changes experienced in great numbers under operating conditions during their lifetime of 25–30 years. Consequently, thermal cycling tests are included in the IEC 61215:2005-standard procedure. It was, therefore, decided to measure the linear coefficient of thermal expansion (CTE) of the front-cover/backsheet core sandwiches. Since the usage of typical aluminium profiles for the module fixing systems was assumed, measures to prevent overstressing due to CTE mismatch could be found this way. The knowledge of the CTEs is also desirable, e.g. when gluing is considered as fixing technique. Results of dilatometric (DIL) analysis according to formula (2) are presented beneath. Fig. 10 illustrates the shape of $dL/L_0 = f(T)$-function (solid line) and its time-derivative (dashed line) for the front-cover/EPGC202 sandwich.

Notice that below the STC-mark the heating process was not controlled by sample temperature and corresponding data were not analysed. From linear segments of the dL/L_0-curve two values of CTE, $\propto_I$ and $\propto_{II}$ (see Table 2) were obtained, this change being assigned to a phase change in the sample at ca. 79°C (the T_1 temperature). Analogous results for the front-cover/CFP sandwich are shown in Fig. 11.

Here, an initial increase in sample length is detected followed by a pronounced decrease below the L_0, the latter seen as a sintering step with T_{onset} of ca. 67°C. Next, a second two-slope increase is observed up to the end of the heating cycle. Corresponding values of CTE are given in

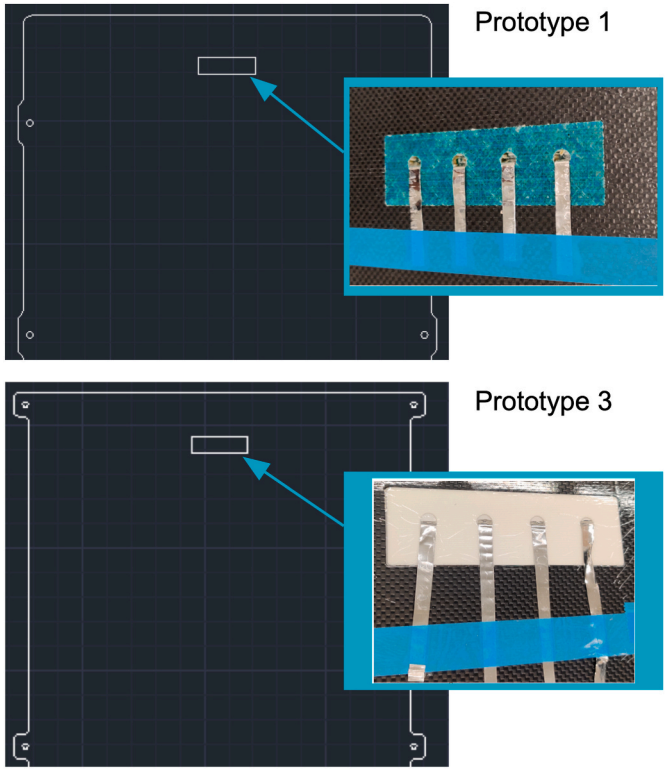

Fig. 18. Location and photographs of insulating inserts: (a) made of GF-N-GF in prototype P1 and (b) of EPGC202 in prototype P3.

Table 2. The sample was then cooled down to 30°C, with results depicted in Fig. 12.

Accordingly, the sample length decreased monotonically, significantly below the L_0, again with $\propto_I$ and $\propto_{II}$. Note that the phase change at ca. 132°C (T_{p2}) corresponds to that of Fig. 11 seen there at ca. 137°C (T_{p1}).

The flexibility of the Nomex® HC cores prevented reliable examination, but sandwiches' linear CTEs are dominated by fibres reinforcing the outer layers: carbon (CF-N-CF) or glass (GF-N-GF), here unspecified. For carbon-fibre composites, the CTEs between -1.6×10^{-6} and -1.0×10^{-6} K^{-1} are quoted in Ref. [54] for polyacrylonitrile- (PAN) and mesophase-based fibres. The anisotropic CTEs were in turn determined for carbon fibre/epoxy composites with different fibre weaves, of -0.76×10^{-6}, $2.97 \times 10^{-6}$and 4.02×10^{-6} K^{-1}, parallel to fibre strands. In measurements taken perpendicular to the fibres, values between 35×10^{-6} and 57×10^{-6} K^{-1} were obtained, similar to those of pure-resin samples [55]. In the same paper the axial CTEs of -0.4×10^{-6} K^{-1} and -1.4×10^{-6} K^{-1} as well as the transverse 5.6×10^{-6} and 3.8×10^{-6} K^{-1} for PAN and pitch fibres were quoted. Note that the values for directions parallel to fibres are consistent with those for the front-cover/CFP sample of Table 2. Regarding the epoxy-glass-fibre composites, the CTE as high as 13.5×10^{-6} K^{-1} was obtained when measured parallelly to fabric reinforcement [56]. Later on, the CTEs of 55×10^{-6} and 15×10^{-6} K^{-1} were measured, respectively, for directions perpendicular and parallel to fibreglass layers [57].

The thermally-induced dimension changes of aluminium support profiles and backsheets should be compensated to avoid modules' overstressing. This is observed when linear CTEs of the backsheets of prototypes P3 and P4 (Table 2) are compared with those of aluminium and duralumin being respectively of 23.6×10^{-6} [58] and 23×10^{-6} K^{-1} [54]. Similar conclusion can be drawn for prototypes P1 and P2 when values for epoxy composites with carbon- and glass-fibres are considered. Caution is required for negative CTEs of backsheets

Table 3
The flow and the parameters of the lamination process by prototype model. The "H" and "L" denotes, respectively, the laminator valve settings for the high and low aeration rate of the space above the laminator membrane.

Process parameter		Degassing of the cut-to-size substrate (P1 and P2)	Prototype			
			P1	P2	P3	P4
Top/bottom layer towards the heating plate		n/a	T	T	B	B
Pre-start	Temperature (°C)	100	132	132	125	125
	Pressure over the diaphragm (mbar)	50	50	50	50	50
Step 1	Temperature (°C)	100	132	132	135	135
	Pressure over the diaphragm (mbar)	40	50	50	50	50
	Valve (H/L)	H	H	H	H	H
	Pressure under the diaphragm (mbar)	40	50	50	50	50
	Duration (s)	40	40	40	40	40
Step 2	Temperature (°C)	100	132	132	135	135
	Pressure over the diaphragm (mbar)	40	50	50	50	50
	Valve (H/L)	L	H	H	H	H
	Pressure under the diaphragm (mbar)	40	50	50	50	50
	Duration (s)	900	260	260	180	180
Step 3	Temperature (°C)	100	136	136	143	143
	Pressure over the diaphragm (mbar)	50	500	500	500	500
	Valve (H/L)	L	L	L	L	L
	Pressure under the diaphragm (mbar)	40	50	50	50	50
	Duration (s)	400	40	40	40	40
Step 4	Temperature (°C)	100	135	135	143	143
	Pressure over the diaphragm (mbar)	50	750	750	870	870
	Valve (H/L)	L	L	L	L	L
	Pressure under the diaphragm (mbar)	1000	50	50	50	50
	Duration (s)	35	900	900	800	800
Step 5	Temperature (°C)	n/a	135	135	143	143
	Pressure over the diaphragm (mbar)	n/a	1000	1000	1000	1000
	Valve (H/L)	n/a	H	H	H	H
	Pressure under the diaphragm (mbar)	n/a	1000	1000	1000	1000
	Duration (s)	n/a	35	35	35	35

Note that the positive results of full-cycle IEC 61215–2:2006 procedure described in Section 3.4 provides a confirmation of sufficient adhesion of interfaces in the prototypes. Particularly, the lack of delamination after the 10.13 Damp-heat (1000h) test was a sufficient proof of the proper selection of materials, the construction of prototypes and the correctness of the lamination process.

(carbon-fibre composites) and/or when composite reinforcements are parallel to the fixing profiles.

Because of honeycomb-based multi-material structures of the Nomex® HC laminates, their thermal stability was examined. In Fig. 13 the TG curves and their first derivatives (DTGs) are depicted by solid and dashed lines, the black and red ones representing, respectively, results for CF-N-CF- and GF-N-GF-structures.

For both samples a decrease in weight was observed, it being less than 2% for temperatures up to 240°C which may be attributed to desorption of gases from the sample surfaces and evaporation of moisture and some of the polymeric material's lighter fractions. Fig. 14 presents results of the DSC analysis, with no significant thermal effects for temperatures between 30 and 240°C. The less-pronounced maximum of red line at ca. 180°C (T_g) may be attributed to glass transition in the epoxy-glass sample (GF-N-GF). Other maxima ending at ca. 100°C may in turn represent resorption of gasses, also seen from TG-curves of Fig. 13. During DSC thermal treatment both samples were destroyed, the remaining material melted and charred. The outer layers, however, maintained their original shapes which may suggest that the degradation occurred mainly in the inner (honeycomb) structure.

The structures of both front-cover/backsheet core sandwiches remain unaffected by elevated temperatures what results from their SEM-imaging. Fig. 15 shows outcomes for the Nomex®-CF (Fig. 15a and b) and Nomex®-GF (Fig. 15c and d) interfaces with front cover as obtained before (Fig. 15a and c) and after (Fig. 15b and d) their heating up to. 160°C.

Indeed, in both cases no significant structural changes were induced by heating. The result proves these materials suitable for use as stable backsheets for PV cells within the temperature range.

3.4. Structures of the prototypes

The structures of PV modules are responsible for their mechanical reliability which in turn is crucial for the flawless performance of low-weight systems. Relevant investigations have been widely performed on constructions under development. Particularly, in Refs. [6,9,10] the composite backsheet (skins/adhesive/honeycomb core) and frontsheet (encapsulant/PV cells/polymeric frontsheet) sandwiches were subjected to IEC 61215-2: 2006 thermal cycling and damp-heat tests showing an excellent stability. In the papers [9,10] the IEC hail tests were successfully carried out. Special attention to hail-resistance tests of analogous structures was in turn paid to in paper [59] where a special combination of frontsheet and backsheet structure was tested according to IEC 61215-2: 2006 hail test. A good impact resistance to hailstones, with less than 5% decrease in module power, were achieved.

The careful selection of construction materials is therefore an essential step in the PV module design process. For obvious reasons, the adhesion of layers was the first priority and had to be examined to find the optimal encapsulant-substrate sets. Due to the speed and ease of executing a large number of investigations, the peel-tests were performed while determining the parameters of lamination process. Such a technique was useful for investigating adhesion in the papers [9–11]. It should be noted that the interface adhesion of some EVA/polyolefin elastomers to the substrates used by us turned out to be insufficient. The increase in adhesion was often possible by adjusting the parameters of the lamination process which, however, led to substrate issues. Using peel-tests, we were able to select a film with good adhesion within a reasonable time. Importantly, with those selections, excursions beyond the substrates' processing window were not required.

Tests of mechanical and environmental reliability were performed on final prototypes, covering the full-cycle of IEC procedures. Regarding mechanical reliability/resistance to environmental conditions, the

Table 4
Technical specification (taken from Refs. [65–68]) and Bill of Materials of the prototypes.

General features		Prototype
Length × width × height (mm)	1300 × 830 × 32	P1, P2
	1445 × 840 × 30	P3, P4
Original weight (kg)/(kg/m^2)	3.45/3.19	P1
	3.75/3.47	P2
	3.85/3.38	P3
	4.30/3.77	P4
Current weight*) (kg)/(kg/m^2)	3.31/3.37	P1
	4.14/3.72	P3
Minimum distance between cells (mm)	1	P1, P2
	2	P3, P4
Minimum cells-edge of laminate distance (mm)	20	P1, P2
	10	P3, P4
Minimum distance between any current carrying part and edge of laminate (mm)	10	P1–P4
PV cells		
Single cell area (cm^2)	155.06	P1–P4
Cell technology	IBC	
Cell manufacturer/model type	Sunpower/Gen III E66 Bin Ne3 5″	
Total number of cells/number of cells in series	60/60	P1, P2
	66/66	P3, P4
Number of series strings	1	P1–P4
Bypass diode		
Number of bypass diodes	3	P1–P4
Diode manufacturer/type	SMC/20SQ045	
Interconnection		
Cell connectors manufacturer/material	Gebauer & Griller/Copper plated with Sn62Pb36Ag2	P1–P4
Cell interconnect dimensions (mm)	2 × 0.15	
String connectors manufacturer/material	Luvata/Sunwire SnPb60/40	
String interconnect dimensions (mm)	5 × 0.12	
Solder bonding technique and material	SnPb60/40	
Fluxing agent	Kester Soldering Flux 952S	
Junction box		
Junction box manufacturer/type	Sunter/4Rail PV-ZH009	P1–P4
Junction box fixing adhesive	Dow Corning PV-804	
Cable manufacturer/type	Sunter/Solar cable 2 × 1 m, 4 mm^2	
Connector manufacturer/type	Sunter/1 × MC4 male, 1 × MC4 female	
Bill of Materials (€)/(€/Wp)	630/2.85	P1
	582/2.61	P2
	778/3.26	P3
	487/2.10	P4

*) after changes in construction due to failed dielectric tests (see Section 3.4).

following steps of ICE 61215 should be mentioned: 10.11 Thermal cycling test (50), 10.11 Thermal cycling test (200), 10.12 Humidity freeze test, 10.13 Damp-heat test (1000h), 10.14 Robustness of termination test, 10.15 Wet leakage current test, 10.16 Mechanical load test and 10.17 Hail test.

In the context of prototype structures, the formula for the PV conversion efficiency, η, at STC [60]:

$$\eta = \frac{P_{mp}}{AE} \tag{6}$$

is of crucial importance. Here A denotes the module total area, E – the incident irradiance. Regarding the P_{mp}, the interdigitated back contact (IBC) SUNPOWER® Gen III E66 Si-monocrystalline cells [61] were chosen. Although more expensive, the mono-Si technology offers better cell parameters than other types [62] and the IBC construction with specific energy conversion provides efficiency exceeding 25% [63,64] which is crucial for the target efficiency of 19%. Next, a compromise is mandatory between the beneficial value of A and the rear cover shape/thickness/structure, these determining the module weight and mechanical stability. For this reason, numerous mechanical-load-tests using the IEC 61215:2005 procedure were performed during the development process. The full-sized samples were loaded in cycles, respectively for a total of 3 h on their front and rear sides. The load was increased gradually from 0 to 2400 Pa at a rate of ca. 70 Pa/min. The structures' weight was also controlled to keep it below the assumed 3.5 kg/m^2. As a result, rectangular rear-covers with filleted lugs for mounting screws of Fig. 16 were obtained (the junction boxes are mounted on their rear surfaces).

The optimal structures of the P1–P4 prototypes obtained in the study are depicted in Fig. 17. In all prototypes the PV cell-strings are sandwiched between the front-covers (see Section 3.1) and the encapsulants.

For the P2 prototype, the electrically-insulating composite (GF-N-GF – see Table ***2***) was chosen for the core. The P4 device was also based on an insulating core (EPGC202) of 1 mm-thickness to keep the 3.5 kg/m^2 weight criterion. The investigations revealed, however, that two additional films (forming the strength layer of Fig. 17) were necessary to achieve the backsheet durability in compliance with IEC 61215:2005 load-test. With these configurations both prototypes passed the full-sequence of IEC 61215:2005/IEC 61730–2:2004 procedures [65,66].

Results of the IEC 61215:2005/IEC 61730–2:2004 tests on the P1 device with electrically-conducting core (CF-N-CF – see Table 2) were, however, negative [67]. This was due to insufficient resistance measured between the module inner circuit and external parts/test fixture. Therefore, the P1 original structure was modified by a double-layered insulator seen in Fig. 17. In this study all changes were continuously examined by electroluminescence (EL) technique to detect the electrical breakdowns and changes' impact on the module weight was also checked. The backsheet was also fitted with a core-thick non-conducting insert perforated to let the ribbons through to the junction boxes (Fig. 18a). Additionally, the mounting holes were reinforced with insulating fittings.

For the P3 module an electrical-conductive CFP core from Table 2 was chosen because of the ultra-low-weight and robustness of carbon-fibre laminate. The IEC 61215/IEC 61730 sequence was passed conditionally, with recommended modification of design [68]. Consequently, following analogous study, the insulating structure as for P1 device was attached to both sides of the core. A non-conductive insert (Fig. 18b) and fittings of backsheet mounting holes were also applied.

According to the IEC requirements, the control tests were performed subsequently after individual procedures. Referring to the issue of modules' mechanical reliability (the IEC 61215 10.16 Mechanical load and 10.17 Hail tests), it is worth, therefore, to summarize corresponding outcomes [65–68]. Note that prior to investigations, the P1–P4 devices were visually inspected with a positive result ("No major visual defects"). The summary is as beneath:

(i) 10.16 Mechanical load test (front side testing pressure: 2400 Pa, back side testing pressure: 2400 Pa) with following results of tests/measurements:
- Visual inspection: no major visual defects (P1–P3), EL test shows several cracks of solar cells. Cells stay intact. No major visual defects (P4). Test passed for P1–P4.
- The 10.15 wet leakage current test: passed for P1–P4.
- Total output power loss: 0% (P1), −1.8% (P2), −4% (P3), −5% (P4).

(ii) 10.7 Hail test (reference parameters of spheres: diameter 25 ± 5% mm, weight 7,53 ± 5% g, speed 23 ± 5% m/s) with location of the shots numbered as follows: a corner of the module window, not more than 50 mm from the frame (1), an edge of the module, not more than 12 mm from the frame (2), over the edge of the circuit (3,4), over the circuit near cell interconnets (5,6), near the point of mounting on the circuit (7,8), in the centre of the circuit, farthest from the mounting points (9,10), any point which may prove especially vulnerable to hail impact (11) with following results of tests/measurements:
- Shots 1–11: passed for P1–P4.

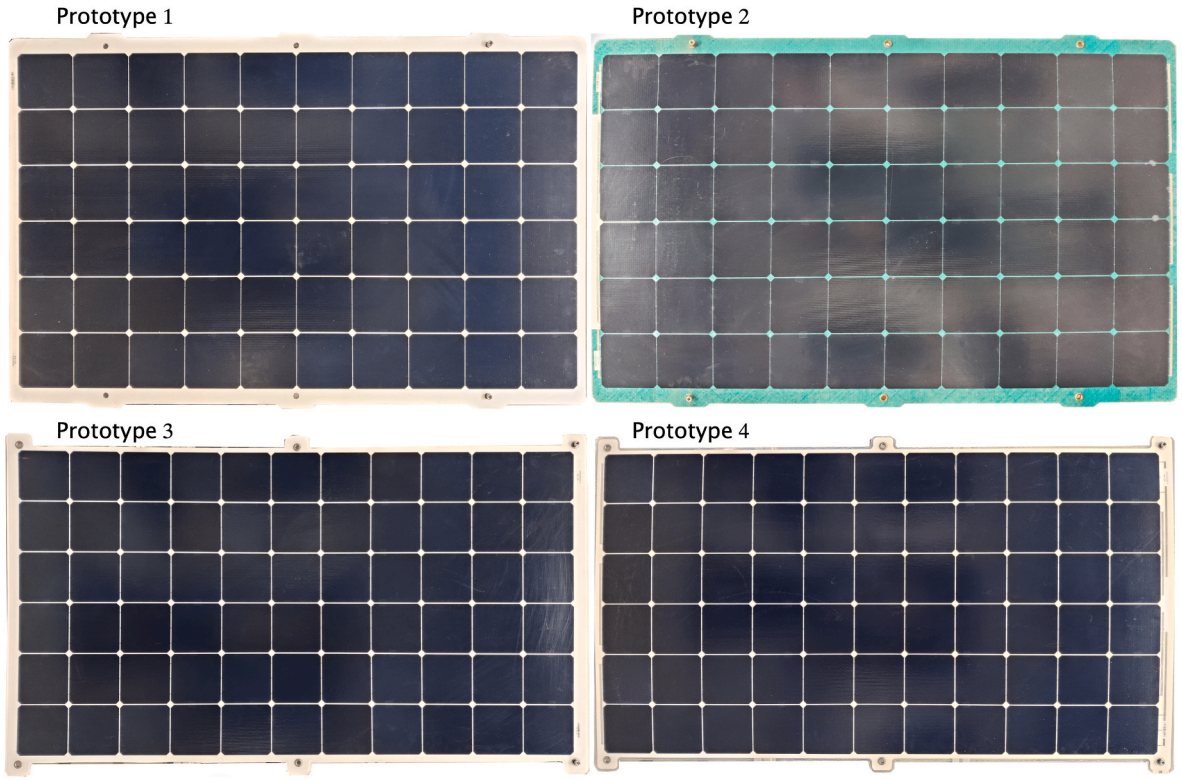

Fig. 19. Photographs of the prototypes.

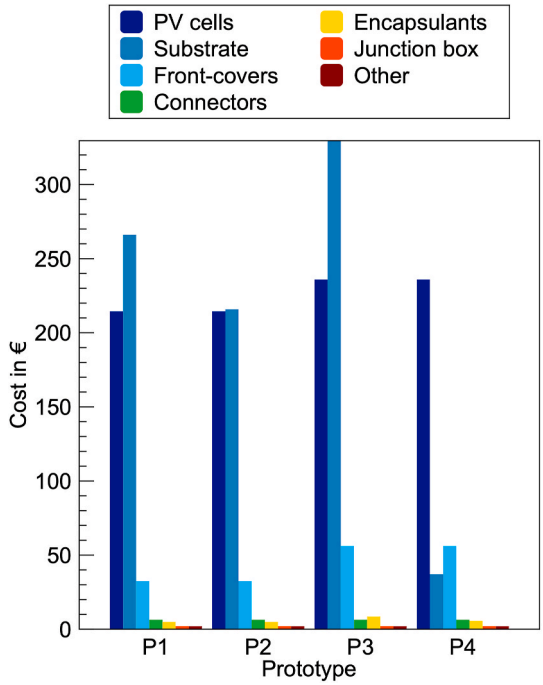

Fig. 20. The costs of components by prototype model.

- Visual inspection: no evidence of major visual defects (P1–P4). Test passed for P1–P4.
- The dielectric withstand test MST 16 (S): passed for P1–P4.

4. Manufacturing of prototypes

In the manufacturing process, the cores were cut according to Fig. 16 using a SERON® 1325 CNC machine and the foils using a ROBUST LQL15 automatic device. Bus-ribbons were prepared by means of an ECOPROGETTI ECOCUT 01B cutting system. The PV cells were manually soldered after a visual quality check by an operator, due to the lack of automatic machinery at that production stage. The honeycomb cut-to-size cores of P1 and P2 prototypes were degassed in a vacuum chamber (100 °C, 1340 s). At a layup station the components were placed on the 3 mm-thick aluminium plates covered with a non-stick ETFE glass-fiber sheet and the layers were lined according to Fig. 17. Additional ETFE mesh was then placed on the layers' top for the texturization of front-covers during lamination. Laminated modules, after cooling down for ca. 15 min., were visually inspected and examined by surface tension tests. As a result of lamination process residual stresses in PV cells emerge [14,16] which can lead to cell damages. The damages lead in turn to reduction of the modules' output power. Such damages can also lead to safety issues which were a subject of our concern in the course of prototype developing process. For this reason, the EL tests were performed on modules to detect the results of structure mechanical stresses. Finally, the modules were trimmed and junction boxes were mounted.

During the development of the lamination process its stages were investigated to eliminate such flaws as e.g. randomly-distributed front-layer shrinkages, formation of gas bubbles and further structures' delamination. An ECOPROGETTI ECOLAM05 MAXI automatic laminator used in Xdisc's regular production was utilized to examine and adjust the parameters of subsequent stages.

The determined six-stage flow and the parameters of the process and step durations are shown in Table 3 by prototype model.

5. Technical parameters and output performance of the prototypes

Basic technical parameters of prototypes are given in Table 4.

The bypass diodes and interconnections were optimized for minimal weight. A series of subsequent peel/EL tests were performed to detect the structure mechanical stresses (see Ref. [16]) to minimize them by applying

Table 5
Averaged values of the short circuit current, I_{sc}, the open circuit voltage, V_{oc}, the V_{mp} and I_{mp} (the voltage and current that determine the maximum power, P_{mp}), the fill factor, *FF*, the conversion efficiency, η, and Power-To-Weight (P2W) ratio by prototype model as obtained from IEC 61215:2005–10.2 tests of P_{mp} at STC taken from Ref. [67] (P1) [65], (P2) [68], (P3) and [66] (P4), together with their standard deviations. Expanded uncertainties, $U(k = 2)$, of measurements are also given for normal probability distribution and level of confidence 95.45% (95.5% for I_{sc}). For irradiation and temperature measurements $U = \pm 30$ W/m^2 and $T = \pm 0.6$°C.

Prototype/#samples	I_{sc}	V_{oc}	V_{mp}	I_{mp}	P_{mp}	*FF*	η	P2W
	A	V	V	A	Wp	%	%	W/kg
P1/8	6.24	43.46	38.36	5.77	221.35	81.63	20.50	66.87
	±0.08	±0.05	±0.16	±0.09	±2.90	±1.56	±0.27	±0.88
P2/8	6.26	43.49	38.31	5.84	223.66	82.13	20.71	59.64
	±0.06	±0.05	±0.16	±0.09	±3.28	±1.73	±0.30	±0.87
P3/9	6.22	48.14	42.63	5.61	238.88	79.78	20.59	57.70
	±0.04	±0.14	±0.32	±0.08	±2.47	±1.40	±0.21	±0.60
P4/8	6.21	47.74	43.00	5.39	231.80	78.00	19.98	53.91
	±0.03	±0.10	±0.25	±0.09	±3.81	±1.56	±0.33	±0.88
U	±0.013	±0.06	±0.30	±0.023	±7.6	±2.8	±0.7	n/a

optimal product type, dimensions of cell/string interconnections and solder bonding technique. As seen, the 3.5 kg/m^2-weight criterion was slightly exceeded for P3 (3.72 kg/m^2) and P4 (3.77 kg/m^2). This is due to the electrically-insulating/strength-improving layers introduced in their structures (cf. Fig. 17). This disadvantage seems to be compensated by the prototype extraordinary durability and aesthetics (P3) or relatively low price (P4). Fig. 19 contains the photographs of the prototypes. Note the eye-pleasing green colour of P2 and the "conventional" white backsheet of remaining ones. The fine module texture was observed to significantly reduce the light reflections.

Table 5 presents the prototypes' electrical output parameters from the IEC 61215:2005–10.2 tests at STC [65–68]. Regarding the project goals, the maximum power, P_{mp} (between ca. 221 and 239 Wp), and conversion efficiency, η (between 19.98 and 20.71%) do exceed the assumed 200 Wp and 19%. The values of the Power-To-Weight (P2W) ratio which is another parameter for comparison of PV modules (see Ref. [69]) are also given. Those are ranged between 54 and 67 W/kg and exceed the 40 W/m^2 reported in this paper for lightweight constructions.

At this stage of the development process, the problem of module cost-effective production arose. Fig. 20 shows that the overall prototype costs (see Table 4) are determined prevailingly by the substrates and cells.

Since materials for the cores were custom-made, their cost in mass-production would decrease significantly according to the manufacturer, especially for prototypes P1 and P3. Another possibility is, e.g. to apply less-expensive substitutes of materials which may need another study. The share of cell prices of ca. 41% (P1), 45% (P2), 37% (P3) and 68% (P4) if high-efficiency (25.4%) PV cells are used were optimized by reduction of P_{mp} and η of the prototypes in statu nascendi to the project-targeted values by application of cheaper PV cells of lowered P_{mp}. This lowered single-cell power, $P_{c,o}$, was determined by Cell-To-Module (CTM) gains and losses analysis of each prototype. The CTM-factors were obtained from formula (4) for given P_{mp} of Table 3 and for the maximum power of a single 25.4%-effective cell, $P_{ci} = 3.94$ Wp [61]. With module effective areas, *A*, of 1.083 (P1, P2) and 1.113 m^2 (P3, P4) the values of $P_{mp,19}$ corresponding to project-targeted η of 19% were determined using formula (6). Finally, the $P_{c,o}$s of 3.66, 3.62, 3.49 and 3.59 Wp were calculated from formula (5), respectively for P1, P2, P3 and P4, these values being related to cell efficiencies of 23.8, 23.5, 22.7 and 23.3% [61]. Consequently, for manufacturing of all prototypes the at least 23.8%-efficient PV cells were chosen to optimize the contract procedures.

6. Conclusions

The paper covers the process of material selection, designing, manufacturing and basic testing of four prototypes of photovoltaic modules for on-grid systems. The study resulted in an adhesively-bonded, frameless construction with a ribbon-interconnected cell matrix sandwiched between frontsheet/encapsulating layers, this structure set-up on a backsheet made of glass- or carbon-fibre reinforced plastic laminates. Commercially available materials were selected and their suitability examined using imaging scanning electron microscopy, analysis of thermal stability and nanoindentation technique. The IBC 5″ Si-monocrystalline PV cells, dedicated backsheets' geometry and sandwich structures were applied. The prototypes' STC-maximum power between 221 and 239 Wp, conversion efficiencies of 19.98–20.71% weight in the range of 3.37 and 3.77 kg/m^2 and Power-To-Weight ratio of 54–67 W/kg were achieved. Hydrophobic foil was used to fabricate the frontsheet/encapsulant films to enhance prototypes' self-cleaning ability. The devices are thus predestined for non-intrusive installations on low-load capacity roofs, even in large-scale lightweight buildings. Limited series of prototypes were manufactured and are the subject to year-long field tests under diverse meteorological conditions of Northern, Central and Southern Poland. Subsequent comparative studies of dismounted devices are planned to address the issue of environmentally induced changes: discolouration (some yellowing of the module sandwiches has been observed so far), delamination, loss of electrical parameters, etc. Our studies were continued in Ref. [70]. In this paper investigations of slightly modified designs (e.g. with reduced cell power due to economic reasons) are described. Particularly, their thermal characterization and performance simulation of PV systems based on the prototypes were conducted. An economic analysis of a system using modified P4-prototype was also performed.

The identified market niche (light-construction buildings e.g. warehouse halls, supermarkets etc.) with enormous economic potential triggered the start of our work on the prototypes and the present paper is to provide examples of solutions that may be useful for the Community in further efforts to satisfy the growing energy needs of the economy.

CRediT authorship contribution statement

Piotr Grygiel: Conceptualization, Methodology, Writing – original draft, Writing – review & editing, Supervision. **Jan Tarłowski:** Conceptualization, Resources, Investigation, Data curation, Validation, Visualization, Funding acquisition. **Marta Prześniak-Welenc:** Investigation, Formal analysis, Visualization, Writing – review & editing. **Marcin Łapiński:** Investigation, Formal analysis, Writing – review & editing, Visualization. **Jacek Łubiński:** Conceptualization, Methodology, Validation, Investigation, Formal analysis, Writing – original draft, Writing – review & editing. **Aleksandra Mielewczyk-Gryń:** Investigation, Formal analysis, Visualization. **Krzysztof Mik:** Conceptualization, Writing – review & editing. **Michał Bartmański:** Investigation, Formal analysis, Visualization. **Daniel Pelczarski:** Investigation, Formal analysis, Visualization. **Maciej Kwiatek:** Investigation, Formal analysis.

Declaration of competing interest

The authors declare that they have no known competing financial interests or personal relationships that could have appeared to influence the work reported in this paper.

Acknowledgements

This work was financially supported by Polish National Center for Research and Development under grant POIR.01.01.01-00-0050/17.

References

[1] IEA, World Energy Outlook 2019, 2019. https://www.iea.org/reports/world-energy-outlook-2019. (Accessed 24 April 2020). accessed.
[2] B. Burger, K. Kiefer, C. Kost, S. Nold, S. Philipps, R. Preu, J. Rentsch, T. Schlegl, G. Stryi-Hipp, H. Wirth, W. Warmuth, Photovoltaics Report, 2019. https://www.ise.fraunhofer.de/content/dam/ise/de/documents/publications/studies/Photovoltaics-Report.pdf. (Accessed 20 May 2020). accessed.
[3] A. Jäger-Waldau, PV Status Report 2019, European Commission, Joint Research Centre, Luxembourg, 2019. https://ec.europa.eu/jrc/en/publication/eur-scientific-and-technical-research-reports/pv-status-report-2019. (Accessed 2 May 2020). accessed.
[4] M. Schmela, et al., Global Market Outlook for Solar Power 2018-2022, 2018. https://www.solarpowereurope.org/wp-content/uploads/2018/09/Global-Market-Outlook-2018-2022.pdf. (Accessed 2 May 2020). accessed.
[5] K. Berger, A.B. Cueli, S. Boddaert, M. Del Buono, V. Delisle, A. Fedorova, F. Frontini, P. Hendrick, S. Inoue, H. Ishii, C. Kapsis, J.-T. Kim, P. Kovacs, N. M. Chivelet, L. Maturi, M. Machado, A. Schneider, H.R. Wilson, International Definitions of BIPV, IEA Photovoltaic Power Systems Programme, 2018. https://iea-pvps.org/key-topics/international-definitions-of-bipv/. (Accessed 11 May 2021). accessed.
[6] A.C. Martins, V. Chapuis, A. Virtuani, H.-Y. Li, L.-E. Perret-Aebi, C. Ballif, Thermo-mechanical stability of lightweight glass-free photovoltaic modules based on a composite substrate, Sol. Energy Mater. Sol. Cells 187 (2018) 82–90, https://doi.org/10.1016/j.solmat.2018.07.015.
[7] C. Olson, B. Geerligs, M. Goris, I. Bennett, J. Clyncke, Current and future priorities for mass and material in silicon PV module recycling, in: Proceedings of the 28th European Photovoltaic Solar Energy Conference and Exhibition, Villepinte, France, 2013, pp. 4629–4633, https://doi.org/10.4229/28thEUPVSEC2013-6BV.8.2.
[8] T. Gorter, A.H.M.E. Reinders, A comparison of 15 polymers for application in photovoltaic modules in PV-powered boats, Appl. Energy 92 (2012) 286–297, https://doi.org/10.1016/j.apenergy.2011.10.042.
[9] A.C. Martins, V. Chapuis, A. Virtuani, C. Ballif, Light and durable: composite structures for building-integrated photovoltaic modules, Prog. Photovoltaics Res. Appl. 26 (2018) 718–729, https://doi.org/10.1002/pip.3009.
[10] A.C. Martins, V. Chapuis, A. Virtuani, C. Ballif, Robust glass-free lightweight photovoltaic modules with improved resistance to mechanical loads and impact, IEEE J. Photovolt. 9 (2019) 245–251, https://doi.org/10.1109/JPHOTOV.2018.2876934.
[11] F. Lisco, A. Virtuani, C. Ballif, Optimisation of the frontsheet encaspulant for increased resistance of lightweight glass-free solar PV modules, in: Proceedings of the 37th European Photovoltaic Solar Energy Conference and Exhibition, on-line conference, 2020, pp. 777–783, https://doi.org/10.4229/EUPVSEC20202020-4BO.11.5.
[12] R. Shivakumara, S.K. Tippabhotla, V.A. Handara, G. Illya, A.A.O. Tay, F. Novoa, R. H. Dauskardt, A.S. Budiman, Fracture mechanics and testing of interface adhesion strength in multilayered structures – application in advanced solar PV materials and technology, Procedia Eng 139 (2016) 47–55, https://doi.org/10.1016/j.proeng.2015.09.232.
[13] T. Kajisa, H. Miyauchi, K. Mizuhara, K. Hayashi, T. Tokimitsu, M. Inoue, K. Hara, A. Masuda, Novel lighter weight crystalline silicon photovoltaic module using acrylic-film as a cover sheet, Jpn. J. Appl. Phys. 53 (2014), 092302, https://doi.org/10.7567/JJAP.53.092302.
[14] A.S. Budiman, S. Anbazhagan, G. Illya, W.J.R. Song, R. Sahay, S.K. Tippabhotla, A. A.O. Tay, Enabling curvable silicon photovoltaics technology using polycarbonate-sandwiched laminate design, Sol. Energy 220 (2021) 462–472, https://doi.org/10.1016/j.solener.2021.03.021.
[15] S. Schindler, D. Götz, D. Dassler, Lightweight PV module approach - field test study and yield evaluation, in: Proceedengs of the 36th European Photovoltaic Solar Energy Conference and Exhibition, France, Marseille, 2019, pp. 54–57, https://doi.org/10.4229/EUPVSEC20192019-1BO.9.5.
[16] W.J.R. Song, S.K. Tippabhotla, A.A.O. Tay, A.S. Budiman, Numerical simulation of the evolution of stress in solar cells during the entire manufacturing cycle of a conventional silicon wafer based photovoltaic laminate, IEEE J. Photovolt. 8 (2018) 210–217, https://doi.org/10.1109/JPHOTOV.2017.2775158.
[17] J. Tracy, N. Bosco, F. Novoa, R. Dauskardt, Encapsulation and backsheet adhesion metrology for photovoltaic modules, Prog. Photovoltaics Res. Appl. 25 (2017) 87–96, https://doi.org/10.1002/pip.2817.
[18] J.T. Simpson, S.R. Hunter, T. Aytug, Superhydrophobic materials and coatings: a review, Rep. Prog. Phys. 78 (2015), 086501, https://doi.org/10.1088/0034-4885/78/8/086501.
[19] W.C. Oliver, G.M. Pharr, An improved technique for determining hardness and elastic modulus using load and displacement sensing indentation experiments, J. Mater. Res. 7 (1992) 1564–1583, https://doi.org/10.1557/JMR.1992.1564.
[20] A.M. Gabor, M. Ralli, K. Gray, Textured glass and antireflective-coated glass for string ribbon PV modules, in: Proceedings of the 22nd European Photovoltaic Solar Energy Conference, Milan, Italy, 2007, pp. 2728–2730.
[21] P. Grunow, D. Sauter, V. Hoffmann, D. Huljić, B. Litzenburger, L. Podlowski, The influence of textured surfaces of solar cells and modules on the energy rating of PV systems, in: Proceedings of the 20th European Photovoltaic Solar Energy Conference, Barcelona, 2005, pp. 2384–2387.
[22] P. Sánches-Friera, D. Montiel, D. Gil, J.A. Montañez, J. Alonso, Daily power output increase of over 3% with the use of structured glass in monocrystalline silicon PV modules, in: Proceedings of the IEEE 4th World Conference on Photovoltaic Energy Conversion, Waikoloa, Hawaii, 2006, https://doi.org/10.1109/WCPEC.2006.279932.
[23] H. Wirth, K.-A. Weiß, C. Wiesmeier, Photovoltaic Modules: Technology and Reliability, first ed., Walter de Gruyter GmbH Berlin/Boston, 2016.
[24] A. Omazic, G. Oreski, M. Halwachs, G.C. Eder, C. Hirschl, L. Neumaier, G. Pinter, M. Erceg, Relation between degredation of polymeric components in crystalline silicon PV module and climatic conditions: a literature review, Sol. Energy Mater. Sol. Cells 192 (2019) 123–133, https://doi.org/10.1016/j.solmat.2018.12.027.
[25] M. Köntges, S. Kurtz, C. Packard, U. Jahn, K.A. Berger, K. Kato, T. Friesen, H. Liu, M. Van Iseghem, Review of Failures of Photovoltaic Modules, International Energy Agency, Photovoltaic Power Systems Programme, 2014. https://iea-pvps.org/wp-content/uploads/2020/01/IEA-PVPS_T13-01_2014_Review_of_Failures_of_Photovoltaic_Modules_Final.pdf.
[26] A. Sayyah, M.N. Horenstein, M.K. Mazumder, Energy yield loss caused by dust deposition on photovoltaic panels, Sol. Energy 107 (2014) 576–604, https://doi.org/10.1016/j.solener.2014.05.030.
[27] M.R. Maghami, H. Hizam, C. Gomes, M.A. Radzi, M.I. Rezadad, S. Hajighorban, Power loss due to soiling on solar panel: a review, Renew. Sustain. Energy Rev. 59 (2016) 1307–1316.
[28] Y.N. Chanchangi, A. Ghosh, S. Sundaram, T.K. Mallick, An analytical indoor experimental study on the effect of soiling on PV, focusing on dust properties and PV surface material, Sol. Energy 203 (2020) 46–68, https://doi.org/10.1016/j.solener.2020.03.089.
[29] B. Weber, A. Quiñones, R. Almanzab, M.D. Duran, Performance reduction of PV systems by dust deposition, Energy procedia 57 (2014) 99–108.
[30] J. Zorrilla-Casanova, M. Piliougine, J. Carretero, P. Bernaola, P. Carpena, L. Mora-López, M. Sidrach-de-Cardona, Analysis of dust losses in photovoltaic modules, in: Proceedings of the World Renewable Energy Congress, Linköping, Sweden, 2011. https://www.researchgate.net/publication/259811727_Analysis_of_Dust_Losses_in_Photovoltaic_Modules.
[31] C. Schill, S. Brachmann, M. Koehl, Impact of soiling on IV-curves and efficiency of PV-modules, Sol. Energy 112 (2015) 259–262, https://doi.org/10.1016/j.solener.2014.12.003.
[32] E. Klugmann-Radziemska, Degradation of electrical performance of a crystalline photovoltaic module due to dust deposition in northern Poland, Renew. Energy 78 (2015) 418–426, https://doi.org/10.1016/j.renene.2015.01.018.
[33] K.-Y. Law, Definitions for hydrophilicity, hydrophobicity, and superhydrophobicity: getting the basics right, J. Phys. Chem. Lett. 5 (2014) 686–688, https://doi.org/10.1021/jz402762h.
[34] Aluminium Feron GmbH & Co, Frontsheet transluX EC 100 Product Information, 2020.
[35] F. Sallaberry, A. Fernández-García, E. Lüpfert, A. Morales, G. San Vicente, F. Sutter, Towards standardized testing methodologies for optical properties of components in concentrating solar thermal power plants, AIP Conf. Proc. 1850 (2016) 150004-1–150004–9, https://doi.org/10.1063/1.4984533.
[36] Specialized Technology Resources, Inc., Technical data of PHOTOCAP® 15585P HLT™, 2015.
[37] K. Gawlińska, K. Drabczyk, Z. Starowicz, P. Sobik, B. Drabczyk, P. Zięba, Determination of eva cross-linking degree after lamination process by extraction and optical transmission measuring, Arch. Metall. Mater. 63 (2018) 833–838, https://doi.org/10.24425/122411.
[38] B.-M. Chen, C.-Y. Peng, G.A. Porter, Optimization of solar module encapsulant lamination by optical constant determination of ethylene-vinyl acetate, Int. J. Photoenergy 1–7 (2015) (2015), 276404, https://doi.org/10.1155/2015/276404.
[39] S.I.N. Ayutthaya, J. Wootthikanokkhan, Investigation of the photodegradation behaviors of an ethylene/vinyl acetate copolymer solar cell encapsulant and effects of antioxidants on the photostability of the material, J. Appl. Polym. Sci. 107 (2008) 3853–3863, https://doi.org/10.1002/app.27428.
[40] A.W. Czanderna, F.J. Pern, Encapsulation of PV modules using ethylene vinyl acetate copolymer as a pottant: a critical review, Sol. Energy Mater. Sol. Cells 43 (1996) 101–181, https://doi.org/10.1016/0927-0248(95)00150-6.
[41] P. Klemchuk, E. Ezrin, G. Lavigne, W. Holley, J. Galica, S. Agro, Investigation of the degradation and stabilization of EVA-based encapsulant in field-aged solar energy modules, Polym. Degrad. Stabil. 55 (1997) 347–365.
[42] J. Jin, S. Chen, J. Zhang, UV aging behaviour of ethylene-vinyl acetate copolymers (EVA) with different vinyl acetate contents, Polym. Degrad. Stabil. 138 (2017) 182–191, https://doi.org/10.1016/j.polymdegradstab.2010.02.020.
[43] B. Ottersböck, G. Oreski, G. Pinter, Comparison of different microclimate effects on the aging behavior of encapsulation materials used in photovoltaic modules, Polym. Degrad. Stabil. 138 (2017) 182–191, https://doi.org/10.1016/j.polymdegradstab.2017.03.010.

[44] E. Kaplani, Degradation effects in sc–Si PV modules subjected to natural and induced ageing after several years of field operation, J. Eng. Sci. Technol. 5 (2012) 18–23.
[45] Djamel E. Mansour, F. Swientek, I. Kaaya, D. Philipp, L.P. Bauermann, Nanoindentation analysis of PV module polymeric components after accelerated aging, in: Proceedings of the 35th European Solar Conference and Exhibition, Brussels, Belgium, 2018, pp. 1333–1336, https://doi.org/10.4229/35thEUPVSEC20182018-5CV.3.28.
[46] T. Sawa, Correlation between nanoindentation test result and Vickers hardness, in: Proceedings of the IMEKO 2010 TC3, TC5 and TC22 Conferences Metrology in Modern Context, Pattaya, Chonburi, Thailand, 2010, pp. 171–174.
[47] M.F. Ashby (Ed.), Materials and the Environment, second ed., Butterworth-Heinemann, 2013.
[48] K. Agrouia, G. Collins, Determination of thermal properties of crosslinked EVA encapsulant material in outdoor exposure by TSC and DSC methods, Renew. Energy 63 (2014) 741–746, https://doi.org/10.1016/j.renene.2013.10.013.
[49] A. Nositschka, D. Neumann, M.-O. Prast, K. Werner, M. Neander, Outdoor monitoring of antireflective and textured cover glasses for solar modules at different sites in Germany, Spain and China of up to 3 years, in: Proceedings of the 24th European Photovoltaic Solar Energy Conference, Hamburg, Germany, 2009, pp. 3359–3362, https://doi.org/10.4229/24thEUPVSEC2009-4AV.3.20.
[50] S.R. Williams, T.R. Betts, R. Gottschalg, D. Neumann, M.-O. Prast, A. Nositschka, Evaluating the outdoor performance of PV modules with different glass textures, in: Proceedings of the 26th European Photovoltaic Solar Energy Conference, Hamburg, Germany, 2011, pp. 3152–3156, https://doi.org/10.4229/26thEUPVSEC2011-4CO.7.3.
[51] Jacek Wróblewski, Effect on Top Layer Geometry on Maximim Power Directional Characteristic of a Photovoltaic Cell, MSc thesis, Gdańsk University of Technology, 2020.
[52] E.K. Masterplatex, Technical Datasheet of Carbon CF-Epoxy Sheets, 2021. https://www.masterplatex.de. (Accessed 10 August 2021). accessed.
[53] IZO-ERG, Technical data of glass sheets. https://www.izoerg.com.pl/for-construction.html, 2021. (Accessed 11 August 2021) accessed.
[54] D.D.L. Chung (Ed.), Carbon Fiber Composites, Butterworth-Heinemann, 1994.
[55] A. Ahmed, B. Tavakol, R. Das, R. Joven, P. Roozbehjavan, B. Minaie, Study of Thermal Expansion in Carbon Fiber Reinforced Polymer Composites, 2012. https://www.researchgate.net/publication/262006977_Study_of_Thermal_Expansion_in_Carbon_Fiber_Reinforced_Polymer_Composites.
[56] G.L. Denman, Thermal Expansion of Reinforced Composites - Thermal Hysteresis Effect, Air Force Materials Laboratory Research and Technology Division , Air Force Systems Command, Wright-Patterson Air Force Base, Ohio, USA, 1966.
[57] D.L. McElroy, F.J. Weaver, C. Bridgman, Thermal expansion of epoxy-fiberglass composite specimens, Int. J. Thermophys. 9 (1988) 233–243, https://doi.org/10.1007/BF00504243.
[58] J.R. Davis (Ed.), Metals Handbook Desk Edition, 2 nd, ASM International, 1998.
[59] A.C. Martins, V. Chapuis, A. Virtuani, L.-E. Perret-Aebi, C. Ballif, Hail resistance of composite-based glass-free lightweight modules for building integrated photovoltaics applications, in: Proceedings of the 33rd European Photovoltaic Solar Energy Conference and Exhibit, The Netherlands, Amsterdam, 2017, pp. 2604–2608, https://doi.org/10.4229/EUPVSEC20172017-6BV.3.62.
[60] A. Luque, S. Hegedus (Eds.), Handbook of Photovoltaic Science and Engineering, John Wiley & Sons Ltd, Chichester, England, 2003.
[61] Sunpower Corp, Technical Product Datasheet of Maxeon Gen III Solar Cells, 2017.
[62] T. Oku, Solar Cells and Energy Materials, Walter de Gruyter GmbH Berlin/Boston, 2017.
[63] C. Battaglia, A. Cuevas, S. De Wolf, High-efficiency crystalline silicon solar cells: status and perspectives, Energy Environ. Sci. 9 (2016) 1552–1576, https://doi.org/10.1039/c5ee03380b.
[64] M.A. Green, E.D. Dunlop, D.H. Levi, J. Hohl-Ebinger, M. Yoshita, A.W.Y. Ho-Baillie, Solar cell efficiency tables (version 54), Prog. Photovoltaics Res. Appl. 27 (2019) 565–575.
[65] A. Ärnström, T. Bergqvist, Q. Daniel, Photovoltaic Module Prototyp 2 Test Report No R00056 rev.00, Midsummer AB, Elektronikhöjden, vol. 6, Unpublished results, Järfälla, Sweden, 2019, p. 175 43.
[66] A. Ärnström, T. Bergqvist, Q. Daniel, Photovoltaic Module Prototyp 4 Test Report No R00057 rev.00, Midsummer AB, Elektronikhöjden, vol. 6, Unpublished results, Järfälla, Sweden, 2019, p. 175 43.
[67] A. Ärnström, T. Bergqvist, Q. Daniel, Photovoltaic Module Prototyp 1 Test Report No R00055 rev.00, Midsummer AB, Elektronikhöjden, vol. 6, Unpublished results, Järfälla, Sweden, 2019, p. 175 43.
[68] A. Ärnström, T. Bergqvist, Q. Daniel, Photovoltaic Module Prototyp 3 Test Report No R00058 rev.00, Midsummer AB, Elektronikhöjden, vol. 6, Unpublished results, Järfälla, Sweden, 2019, p. 175 43.
[69] S. Schindler, D. Götz, J. Schneider, Beyond watt per module and costs per watt – new weight related parameters for photovoltaic modules, in: Proceedings of the 35th European Photovoltaic Solar Energy Conference and Exhibition, Brussels, Belgium, 2018, pp. 1790–1793, https://doi.org/10.4229/35thEUPVSEC20182018-6BV.1.27.
[70] K. Mik, P. Zawadzki, J. Tarłowski, M. Bugaj, P. Grygiel, S. Bykuć, Multifaceted analyses of four different prototype lightweight photovoltaic modules of novel structure, Energies 14 (2021) 1–16, https://doi.org/10.3390/en14082239.